THE JOURNAL OF PHYSICAL CHEMISTRY C

Article

pubs.acs.org/JPCC

pH and Alkali Cation Effects on the Pt Cyclic Voltammogram Explained Using Density Functional Theory

Ian T. McCrum and Michael J. Janik*

Department of Chemical Engineering, The Pennsylvania State University, 104 Fenske Laboratory, University Park, Pennsylvania 16802, United States

Supporting Information

ABSTRACT: Platinum electrode cyclic voltammograms show features at low potentials which correspond to adsorption/desorption processes on Pt(111), Pt(100), and Pt(110) facets that have traditionally been ascribed to hydrogen adsorption. The 100 and 110 associated features exhibit a dependence on pH beyond the expected Nernstian shift. Herein we use density functional theory (DFT) to explain these shifts. We examine the specific adsorption of hydrogen, hydroxide, water, and potassium onto the low index facets of platinum, Pt(111), Pt(100), and Pt(110). In support of a growing body of evidence, we show that the low potential features which correspond to adsorption/desorption on Pt(100) and Pt(110) contain contributions from the competitive or coadsorption of hydroxide. This allows us to simulate cyclic voltammograms for Pt(100) and Pt(110), as well as Pt(111), which match experimentally measured cyclic voltammograms in a pH = 0 electrolyte. Furthermore, we find that potassium cations can specifically adsorb to all three low index facets of platinum, weakening the binding of hydroxide. As potassium-specific adsorption becomes more favorable with increasing pH, this allows us to explain the measured pH dependence of these features and to simulate cyclic voltammograms for the three low index facets of platinum which match experiment in a pH = 14 electrolyte. This has significant implications in catalysis for hydrogen oxidation/evolution, as well as for any electrocatalytic reaction which involves adsorbed hydroxide.

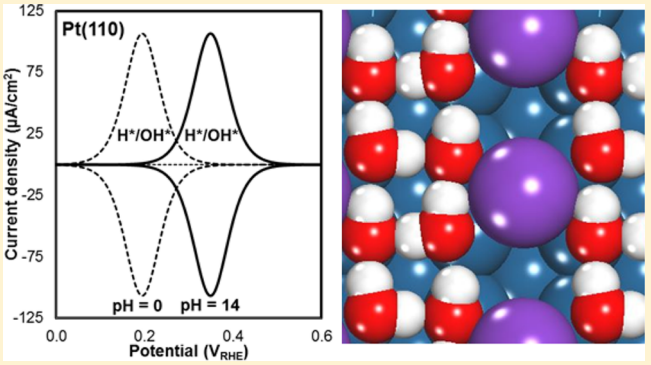

INTRODUCTION

Adsorption of hydrogen (H^+) and hydroxide (OH^-) onto platinum electrodes forms reactive surface intermediates involved in many electrocatalytic reactions, including hydrogen oxidation and evolution,[1−4] oxygen reduction and evolution,[5−7] CO oxidation and stripping,[8−11] and methanol oxidation.[8,12] However, the thermodynamics of hydrogen and hydroxide adsorption onto platinum in an electrochemical environment, as examined by cyclic voltammetry, are still debated. Changes in pH give an unexplained shift in the thermodynamics of hydrogen and hydroxide adsorption, beyond the Nernstian shift expected due to the change in concentration/activity of hydrogen and hydroxide. In this work we examine the effects of pH and the presence of a specifically adsorbed alkali metal cation, potassium, on the adsorption of protons, hydroxide, and water onto platinum electrode surfaces.

Polycrystalline platinum electrodes show three pronounced features in cyclic voltammograms within the 0−0.5 V_{RHE} (reversible hydrogen electrode) range.[4,13] A series of single-crystal electrode cyclic voltammetry studies, including the three low index platinum facets, have facilitated assigning these peaks to the 111, 100, and 110 facets, and they are typically referred to as hydrogen adsorption/desorption features.[4,14−16] Higher-order facets can readily be deconvoluted to contributions from flat 111 terraces and contributions from 100 and 110 steps.[16,17] The width of the terrace in the higher-order facets has only a minor effect on adsorption, though there are subtle differences in the shape of low potential features between 110 steps on high-order facets with wide terraces,[17] those with short terraces (Pt(211)[18]), and the low index Pt(110) facet.[14,15] Ultrahigh vacuum studies support this deconvolution to contributions from steps and terraces on higher-order platinum facets, at least for hydrogen and oxygen adsorption.[19−21]

While these low potential features in cyclic voltammograms on platinum have traditionally been thought to be due to hydrogen adsorption/desorption, a growing body of evidence strongly suggests that hydroxide adsorption also contributes to these features on all platinum surfaces except for Pt(111) (and 111 terraces). This competitive or coadsorption of hydrogen and hydroxide on Pt(100), Pt(110), and Pt steps seems intuitive given the expected stronger binding of hydrogen and hydroxide to these lower coordinated surfaces. The Feliu group[22] has previously used the coadsorption of H and OH on platinum steps to explain the magnitude and shape of these low

Received: November 9, 2015
Revised: December 10, 2015

DOI: 10.1021/acs.jpcc.5b10979
J. Phys. Chem. C XXXX, XXX, XXX−XXX

potential features measured in acid.[22] CO displacement experiments, which give a significantly lower potential of zero charge for stepped platinum surfaces than for Pt(111), further corroborate this competitive adsorption, suggesting hydroxide adsorption can occur at lower potentials on steps than on Pt(111).[23−28] Rigorous thermodynamic analyses performed by Garcia-Araez et al.[15,29] and Gómez et al.[14] show that these features can be deconvoluted into contributions from hydrogen adsorption and contributions from hydroxide adsorption on Pt(100) and Pt(110) electrodes.

Recent density functional theory (DFT) calculations have shown that the free energy to dissociate adsorbed water to coadsorbed hydrogen and hydroxide is positive on Pt(111) but negative on Pt(100), Pt(110), and Pt steps,[30−32] showing it is thermodynamically favorable to coadsorb hydrogen and hydroxide on these surfaces. Kolb et al. showed stronger binding for H, OH, and water on the Pt(100) step edge and stronger binding for OH on the Pt(110) step edge relative to Pt(111), though they neglect the effect of coadsorbed water, which would act to stabilize adsorbed OH and further promote water dissociation.[33] In contrast to these findings, Karlberg et al. use DFT to model cyclic voltammograms for hydrogen adsorption on Pt(111) and Pt(100) electrode surfaces that match experiment well, even though hydroxide competitive adsorption on Pt(100) is neglected.[34] The involvement of hydroxyl adsorption in these low potential features, therefore, remains unclear.

The low potential features measured by cyclic voltammetry on Pt(100), Pt(110), and Pt steps show a dependence on pH beyond the expected Nernstian shift,[4,17] which has yet to be explained. The broad peak associated with hydrogen adsorption on Pt(111) is relatively pH independent, experiencing only the Nernstian shift corresponding to the change in concentration of protons, leaving the peak unaltered on a RHE scale.[17] van der Niet et al. showed that, on well-defined single-crystal electrodes, the low potential feature on stepped platinum electrodes is at a lower potential in acid than in base on an RHE scale (where the Nernstian shift is already accounted for).[17] The low potential feature for facets which contain (110) or (100) steps both shift by ∼10 mV_{RHE}/pH unit.[17] The broad low potential peak on Pt(111) remains unchanged by pH, though the high potential (111) associated hydroxide adsorption peak changes shape between an acid electrolyte and a basic electrolyte.[17] A similar trend was seen previously in phosphate-containing electrolytes with polycrystalline platinum.[13] Sheng et al. find identical results with polycrystalline platinum, showing two sharp low potential peaks, presumed to correspond to adsorption on Pt(110) and Pt(100), which shift almost linearly with pH.[4] This non-Nernstian shift is important to catalysis, as the location of these peaks on the relative hydrogen electrode scale correlates with the rate of the hydrogen oxidation reaction. A CV peak shift to more positive potentials by ∼0.15 V on increasing the pH from 0 to 13 correlates with a roughly 2 orders of magnitude decrease in the hydrogen oxidation/evolution reaction rate, when compared to the rate measured in acid in an operating PEM fuel cell under conditions free from mass transfer limitations.[4,35,36]

This sub-Nernstian shift has so far gone unexplained. van der Niet et al. proposed that, in alkaline media, relatively more hydroxide may be adsorbed than in acidic media, that the electrosorption valency of hydroxide may not be unity, or that a low coverage of oxygen may be coadsorbed with hydroxide, giving this peak its experimentally measured pH dependence on an RHE scale.[17] It is unclear, however, why the electrosorption valency or ratio of adsorbed hydroxide to adsorbed oxygen would be pH dependent. Sheng et al. suggest that the shift of these low potential peaks with pH could be due to coadsorbed or competitively adsorbed hydroxide but provide no insight into why this competition should be pH dependent on an RHE scale.[4] Sheng et al. assumed this shift was a direct measure of hydrogen binding energy but provide no explanation as to why the binding strength of hydrogen on Pt(100) or (110) would depend on pH.[4] One possible explanation for this shift with pH, not considered previously, is the presence of specifically adsorbed alkali metal cations on the electrode surface as the pH is increased, as alkali cation specific adsorption becomes more favorable relative to proton adsorption with increasing pH.

Alkali metal cation specific adsorption onto platinum electrodes has only limited direct experimental evidence, though recent density functional theory efforts show their adsorption is favorable at high pH and low potential onto Pt(111),[37,38] Pt(100), and Pt(110).[38] Indirect experimental evidence includes radiotracer studies showing sodium and cesium adsorption from alkaline solutions onto platinum electrodes[39] as well as studies showing their coadsorption with various anions, including (bi)sulfate[40−43] and cyanide,[44,45] supported by direct STM imaging and DFT calculations.[44−48] Nanogravimetric electrochemical experiments show the specific adsorption of cesium at low potentials in a sulfuric acid electrolyte as well as its coadsorption with (bi)sulfate.[49,50] A building body of evidence suggests the presence of alkali metal cations effects a variety of electrochemical reactions, including hydrogen oxidation and evolution,[51,52] methanol oxidation,[51,53] formate oxidation,[54] ethylene glycol oxidation,[55−57] CO oxidation and stripping,[58,59] oxygen reduction[51] and evolution,[60,61] and CO_2 electroreduction.[62] It has been unclear, however, whether these effects occur due to specific cation adsorption or influence from nonspecific adsorption of cations in the electrochemical double layer.

Herein, we use density functional theory to examine the specific adsorption of hydrogen, hydroxide, water, and potassium onto Pt(111), Pt(100), and Pt(110) electrode surfaces. We find that hydrogen binds more strongly to Pt(100) and Pt(110) electrodes than to Pt(111), in contrast to experimentally measured cyclic voltammograms which show desorption from Pt(110) at potentials lower than the corresponding peak on Pt(100) and intermediate to the broad peak seen with Pt(111). We then show that adsorption of hydroxide is also much more favorable on Pt(100) and Pt(110) than on Pt(111) and would occur within the traditional "hydrogen adsorption region" on stepped platinum surfaces. This lends concrete thermodynamic evidence to support that these low potential peaks measured on stepped platinum surfaces in cyclic voltammetry correspond to the competitive adsorption of hydrogen and hydroxide. While we only investigate the low index facets of platinum, a significant body of electrochemical results suggest that the behavior of higher-order platinum facets and polycrystalline platinum electrodes can be at least roughly deconvoluted into contributions from the low index facets.[4,16,17]

Furthermore, we find that potassium cations can favorably adsorb to low coverages on Pt(111), Pt(100), and Pt(110) and could compete with hydrogen adsorption in high pH electrolytes. We find specifically adsorbed potassium has no effect on the adsorption energetics of hydrogen but a significant effect on the adsorption of hydroxide. The effect matches the

DOI: 10.1021/acs.jpcc.5b10979
J. Phys. Chem. C XXXX, XXX, XXX−XXX

pH dependence of these low potential peaks measured on stepped or polycrystalline platinum electrodes. As the pH is increased, not only is a countercation such as potassium added to the electrolyte but also the absolute potential of the electrode is lowered, thereby making the reductive potassium specific adsorption more favorable, increasing its coverage on the surface. Coadsorbed potassium disrupts the solvation of adsorbed hydroxide, destabilizing the surface hydroxide and driving the adsorption peak measured in cyclic voltammetry to higher potentials at higher pH. We compare our results with a significant body of both computational and experimental work, including prior DFT simulations and both electrochemical and UHV surface science studies.

METHODS

Computational Details. Density functional theory (DFT) was used to probe the specific adsorption thermodynamics of hydrogen, hydroxide, potassium, and water onto Pt(111), Pt(100), and Pt(110) electrode surfaces. Electronic structure calculations were performed using the Vienna ab initio Simulations Package (VASP),[63−65] using a plane-wave basis set and the Perdew−Wang (PW91) exchange-correlation functional.[66] The Projector Augmented Wave (PAW) approach was used to describe the ion−core interactions.[67,68] A 5 × 5 × 1 Monkhorst−Pack mesh[69] was used to sample k-space for the 3 × 3 and 4 × 4 unit cells, and 7 × 7 × 1 mesh was used for the 2 × 2 unit cells. The cutoff energy for the plane-wave basis set was 450 eV, and the structural optimization was complete when the magnitude of the forces on the atoms was less than 0.02 eV $Å^{-1}$. The DFT energies are converged to within 0.03 eV with respect to the k-space sampling mesh and the plane-wave cutoff energy. Dipole corrections were included in all surface calculations in the surface normal direction (LDIPOL = TRUE, IDIPOL = 3). The experimentally measured Pt lattice constant of 3.92 Å was used.[70] All surface calculations used a 4-layer slab, with the bottom two layers frozen during optimization. An adsorption site preference analysis was performed for each adsorbate alone on each surface at 1/9 ML (in the 3 × 3 unit cell). Results are given in Table S1 of the Supporting Information. K* preferred the 3-fold hollow site on all three facets. H* preferred the FCC site on Pt(111) and bridge site on Pt(100) and Pt(110). OH* preferred atop sites on Pt(111) and Pt(110) and bridge sites on Pt(100). OH* was also modeled with coadsorbed water, with results given in the section "Surface solvation and adsorbed water". Bader charge analysis was performed using the implementation developed by the Henkelman group.[71−73]

Calculating Equilibrium Adsorption Potentials. The procedure for calculating the equilibrium adsorption potentials for alkali metal cations, hydrogen, and anion adsorption has been described previously[37,74,75] and is reviewed here.

The adsorption reaction for an aqueous cation, including a proton and potassium ion, can be written as a reduction reaction

$$* + C^+_{aq} + e^- \rightarrow C^* \quad (1)$$

where * represents a bare surface site, C^+_{aq} and C* the solution phase and surface adsorbed cation, respectively, and e^- an electron from the electrode. Similarly, the adsorption of an anion such as hydroxide can be written as an oxidation reaction

$$* + OH^-_{aq} \rightarrow OH^* + e^- \quad (2)$$

where OH^-_{aq} and OH* represent solution-phase and adsorbed hydroxide, respectively. The Gibbs free energy changes for each adsorption reaction as a function of electrode potential on an absolute scale are

$$\Delta G^{C^+}_{ads}(U_{abs}) = G_{C^*} - G_* - G_{C^+_{aq}} + |e|U_{abs} \quad (3)$$

$$\Delta G^{OH^-}_{ads}(U_{abs}) = G_{OH^*} - G_* - G_{OH^-_{aq}} - |e|U_{abs} \quad (4)$$

for reactions 1 and 2, respectively. $\Delta G^{C^+}_{ads}(U_{abs})$ and $\Delta G^{OH^-}_{ads}(U_{abs})$ are the free energy changes for each respective adsorption reaction, G_{C^*} and G_{OH^*} the free energy of adsorbed cation and adsorbed hydroxide, $G_{C^+_{aq}}$ and $G_{OH^-_{aq}}$ the free energy of the solution-phase cation and hydroxide, respectively, G_* the free energy of a bare surface site, and $|e|U_{abs}$ the free energy of an electron on an absolute potential scale.

The free energy of the adsorbed species X*, G_{X^*}, is calculated as

$$G_{X^*} = E^{DFT}_{X^*} + ZPVE - TS_{vib} \quad (5)$$

where $E^{DFT}_{X^*}$ is the DFT energy of the adsorbed species−surface state, ZPVE the zero-point vibrational energy, and TS_{vib} the vibrational entropy of the surface−adsorbate bond (and of the bonds in the adsorbate, in the case of adsorbed hydroxide). It is assumed that the phonon modes of the metal electrode surface are not perturbed by the adsorbate. The free energy of the surface is therefore calculated as

$$G_* = E^{DFT}_* \quad (6)$$

To calculate the free energy of the solution-phase cations $G_{C^+_{aq}}$ and $G_{H^+_{aq}}$, two different methods are used. The aqueous potassium cation free energy, $G_{K^+_{aq}}$, is calculated by finding the free energy of the cation in the gas phase, accounting for translational entropy, then adding on an experimentally measured solvation energy for the cation in a 1 M solution (ΔG^0_{solv})

$$G_{K^+_{aq}} = E^{DFT}_{K^+_g} - TS_{trans} + \Delta G^0_{solv} \quad (7)$$

The free energy of the aqueous phase proton, $G_{H^+_{aq}}$, is calculated using the computational hydrogen electrode,[76] as given by reaction 8 and eq 9

$$H_{2(g)} \rightarrow 2H^+_{aq} + 2e^- \quad (8)$$

$$G_{H^+_{aq}} = \frac{2eU_0 + G_{H_2}}{2} \qquad U_0 = 0.00V_{NHE}@pH = 0 \quad (9)$$

We find that the solvation energy method described above for finding the free energy of $G_{K^+_{aq}}$ and previously for finding the free energy of an aqueous-phase halide[75] matches the approach of using an experimental dissolution potential to within 0.3 eV. A comparison for the aqueous free energy of K^+ and H^+ calculated using the two methods is given in Table S2 in the Supporting Information.

The free energy of the solution-phase hydroxide, $G_{OH^-_{aq}}$, is calculated using an approach similar to the computational hydrogen electrode method, using the hydrogen oxidation reaction and its known potential in a pH = 14 solution (−0.826 V_{NHE}[76]). The overall reaction is

$$H_{2(g)} + 2OH^-_{aq} \rightarrow 2H_2O_{aq} + 2e^- \quad (10)$$

DOI: 10.1021/acs.jpcc.5b10979
J. Phys. Chem. C XXXX, XXX, XXX−XXX

Since the overall free energy change for this reaction is known, from its equilibrium potential, and the free energies of $H_{2(g)}$ and H_2O_{aq} can easily be calculated, the free energy of the solution-phase hydroxide anion can be found, as given by eq 11

$$G_{OH^-_{aq}} = \frac{2G_{H_2O} - 2eU_0 - G_{H_2}}{2} \quad U_0 = -0.826V_{NHE}@ \; pH = 14 \tag{11}$$

where G_{H_2O} and G_{H_2} are the free energies of solution-phase water and gas-phase hydrogen molecules, respectively. G_{H_2O} and G_{H_2} are calculated by

$$G_{H_2O_{(aq)}} = E^{DFT}_{H_2O_{(g)}} - TS_{gas} + ZPVE + U_{int} + PV \tag{12}$$

$$G_{H_{2(g)}} = E^{DFT}_{H_{2(g)}} - TS_{gas} + ZPVE + U_{int} + PV \tag{13}$$

where TS_{gas} is the translational, rotational, and vibrational entropy of the molecule; ZPVE is the zero-point vibrational energy; U_{int} is the internal energy of the molecule; and PV is the pressure−volume contribution to the gas-phase free energy. $G_{H_2O_{(aq)}}$ is calculated as the free energy of gas-phase water at a partial pressure equal to the vapor pressure of a 300 K aqueous solution (0.035 bar),[76] where $G_{H_2O_{(aq)}} = G_{H_2O_{(g)}}$. Calculated free energies can be found in the Supporting Information.

Finally, eqs 3 and 4 can be expanded to include corrections to the free energy due to the interaction of the surface normal dipole moment with the interfacial electric field, yielding eqs 14 and 15

$$\Delta G^{C^+_{aq}}_{ads}(U_{NHE}) = G_{C^*} - e(U_{NHE} + 4.6) + |e|(U_{NHE} - U_{pzc})\frac{\mu_{C^*} - \mu_*}{d} - G_* - G_{C^+_{aq}} \tag{14}$$

$$\Delta G^{OH^-}_{ads}(U_{NHE}) = G_{(OH)^*} + eU_{NHE} - |e|(U_{NHE} - U_{pzc})\frac{\mu_{(OH)^*} - \mu_*}{d} - G_* - G_{OH^-_{aq}} \tag{15}$$

with $((\mu_{C^*} - \mu_*)/d)$ the change in surface normal dipole moment on adsorption divided by d, the Helmholtz thickness, taken to be 3 Å.[76] The adsorption free energy of the cation, $\Delta G^{C^+_{aq}}_{ads}(U_{NHE})$, is shifted from an absolute to the normal hydrogen electrode scale (NHE) using the 4.6 V difference between scales observed experimentally[77−79] and replicated computationally.[80] This correction is not needed for hydrogen adsorption when using the computational hydrogen electrode as it references the NHE scale.

In all cases the temperature is taken as 300 K and the concentration of each species 1 M unless otherwise noted. All entropic contributions to free energy are calculated using traditional statistical mechanics relationships. Vibrational energy and entropy are calculated using vibrational frequencies calculated by VASP, by computing the Hessian matrix from atomic displacements of 0.01 Å in each Cartesian direction.

To calculate equilibrium adsorption potentials, eqs 14 and 15 are solved for the potential, U_{NHE}, where $\Delta G_{ads} = 0$.

Surface Solvation and Adsorbed Water. Aqueous electrolyte near the electrode surface has little effect on the adsorption of hydrogen[34,37] but can have a significant effect on the adsorption of alkali cations[37] and hydroxide.[18,81]

To model the effect of surface solvation on potassium adsorption, we evaluate the Gibbs free energy change for adsorption of potassium at 1/9 ML on Pt(111), Pt(100), and Pt(110) with one, three, or six explicit water molecules placed near the surface−adsorbate bond. The method used here has been described previously.[37,75] One, three, or six water molecules are placed near potassium on the electrode surface, and the structure is relaxed and the free energy calculated; the potassium atom is then removed, the structure relaxed again, and the free energy of the solvated clean surface calculated. While it is not guaranteed that the global minimum energy water structure is found, this method does not require knowledge of the near-surface water structure, which is long-range and metal surface dependent. Using a small number of explicit water molecules allows for solvation effects on adsorption free energy to be approximated without greatly increasing computational effort. Furthermore, while the free energy calculated here only includes the vibrational energy and entropy of the water structure, thereby neglecting configurational entropy of the dynamic water, we assume the difference in these properties between the initial and final states here to be small. The Gibbs free energy change for potassium cation adsorption onto the solvated electrode surface is calculated in a manner similar to eq 14, shown in eq 16

$$\Delta G^{C^+_{aq}}_{ads}(U_{NHE}) = G_{(H_2O)_nC^*} - e(U_{NHE} + 4.6) + |e|(U_{NHE} - U_{pzc})\frac{\mu_{C^*} - \mu_*}{d} - G_{(H_2O)^*_n} - G_{C^+_{aq}} \tag{16}$$

where $G_{(H_2O)_nC^*}$ is the adsorbed surface state containing 1/9 ML potassium and one, three, or six water molecules, and $G_{(H_2O)^*_n}$ is the solvated bare surface state.

We also model the effect of implicit solvation on the adsorption of potassium at 1/9 ML onto Pt(111), Pt(100), and Pt(110), using the implicit solvation model implemented in VASP by the Hennig and Arias groups.[82] We use the default solvent parameters defined for water[82] with an ENCUT = 800.

To model the effect of adsorbed water on the adsorption of hydroxide on Pt(111) and Pt(100), the minimum energy hydroxide−water coadsorbed structure was found in the prior literature and replicated on a 3 × 3 surface. For Pt(111), the minimum energy structure is a hexagonal arrangement of 1/3 ML OH* and 1/3 ML H_2O* as determined from DFT[83−86] and UHV STM imaging, low energy electron diffraction (LEED), and spectroscopic techniques.[87−89] The minimum energy water structure on Pt(111) was the 2/3 ML ice-like bilayer.[86] For Pt(100), the minimum energy hydroxide and water structure is a square-like alternating arrangement of OH* and H_2O* at 1/3 ML H_2O* and 1/3 ML OH*, and the minimum energy water structure was 2/3 ML H_2O* as determined by DFT.[90] This coverage of OH* on Pt(100) compares well with that found by Gómez et al.[14] and Garcia-Araez et al.[91] in electrochemical cyclic voltammetry in perchloric acid.

For hydroxide and water adsorption on Pt(110), no known minimum energy structure could be found. As it is well-known that the minimum energy structure of adsorbed hydroxide and water on platinum maximizes the number of hydrogen bonds between OH* and H_2O*,[83] two structures were considered: an alternating square arrangement of 1/3 ML H_2O* and 1/3 ML OH* in a 3 × 3 unit cell and an alternating square arrangement of 1/2 ML H_2O* and 1/2 ML OH* in a 2 × 2 unit cell. 1/2

DOI: 10.1021/acs.jpcc.5b10979
J. Phys. Chem. C XXXX, XXX, XXX−XXX

ML H_2O^* and 1/2 ML OH* in a 2 × 2 unit cell were found to be lower in energy (per OH*).

The free energy to adsorb or form hydroxide in these minimum energy structures (MES) of coadsorbed hydroxide and water is calculated by removing half of the hydrogen atoms, as protons, from an adsorbed water layer to form the coadsorbed hydroxide and water layer. This hydroxide formation free energy is given in eq 17.

$$G^{OH^-}_{ads,MES}(U_{NHE}) = G_{(H_2O)_{n-x}OH^*_x} + xeU_{NHE} + xeU_{NHE} \frac{\mu_{(OH)^*} - \mu_*}{d} - G_{(H_2O)_n*} + xG_{H^+_{aq}} \quad (17)$$

$G_{(H_2O)_{n-x}OH^*_x}$ is the free energy of the coadsorbed hydroxide and water structure, $G_{(H_2O)_n*}$ the free energy of the adsorbed water reactant structure, and x the number of protons/electrons removed.

To further investigate the effect of coadsorbed water on hydroxide adsorption, the adsorption of hydroxide on each of the three facets was also investigated at low coverage (1/9 ML) with 1 coadsorbed water molecule. The free energy of adsorption is then calculated as given by eq 18, equivalent to eq 16:

$$\Delta G^{OH^-}_{ads}(U_{NHE}) = G_{(H_2O)_nOH^*} + eU_{NHE} + eU_{NHE} \frac{\mu_{(OH)^*} - \mu_*}{d} - G_{(H_2O)_n*} - G_{OH^-_{aq}} \quad (18)$$

eq 17 differs from eq 18 in that protons are desorbed from the water structure instead of hydroxide adsorbed into the water structure. Both methods are equivalent, assuming the pH used is the same in each case, and only differ in the stoichiometry used in the explicit solvation shell.

While the absolute energy and free energy change of adsorption will certainly depend on the particular water structure evaluated, both for water adsorbed onto and near the electrode surface, we find that the trend in adsorption across facets or with coadsorbed alkali cations is independent of water structure and holds even when only one water molecule solvates the electrode surface.

Images of all water and coadsorbed hydroxide and water structures on each of the three facets are given in the Supporting Information. A comparison of the different approaches for calculating the hydroxide adsorption free energy is given in the Supporting Information.

Quantifying Adsorbate−Adsorbate Interactions. To quantify the interaction between one adsorbate and another on the same surface, the free energy of "interaction" is calculated using the following reaction

$$X_1^* + X_2^* = (X_1X_2)^* + * \quad (19)$$

where X_1^* and X_2^* are independent adsorbates, and $(X_1X_2)^*$ represents the two species adsorbed in the same surface unit cell. The free energy change for this reaction is simply

$$\Delta G_{X_1-X_2} = G_{(X_1X_2)^*} + G_* - G_{X_1^*} - G_{X_2^*} \quad (20)$$

where a positive $\Delta G_{X_1-X_2}$ describes a repulsive X_1-X_2 adsorbate interaction.

Computational Cyclic Voltammograms. Cyclic voltammograms for adsorption of ionic species were modeled by solving for the rate of adsorption with electron transfer as a function of potential, scan rate, and species coverage under the assumption that adsorption is equilibrated at all potentials. This approach has been previously described for modeling the CV features associated with (bi)sulfate adsorption.[74] The equilibrium constant for adsorption of an ionic species, X, can be written as

$$K_{X^*}(U, \theta_{X^*}) = \exp\left(\frac{-\Delta G_{X^*}(U, \theta_{X^*})}{RT}\right) = \frac{\theta_{X^*}}{\theta_* a_{X(aq)}} \quad (21)$$

where θ_{X^*} is the coverage of adsorbed species X; θ_* is the coverage of bare or unoccupied surface sites; $a_{X(aq)}$ is the activity of ionic species X in solution; R is the gas constant; T is the temperature; and $\Delta G_{X^*}(U, \theta)$ is the Gibbs free energy of adsorption of species X to the electrode surface as a function of its coverage and the electrode potential U. The potential (U) is defined as a function of time, t, and scan rate, ν, from an initial starting potential U_0

$$U = U_0 + \nu t \quad (22)$$

Finally the voltammetric current density due to adsorption of species X can be written as

$$j_{X^*} = \left(\frac{m \times e}{A}\right)\frac{d\theta_{X^*}}{dt} \quad (23)$$

where m is the maximum coverage and A is the area of the unit cell. The cyclic voltammograms are each simulated at a scan rate of 50 mV/s and a surface atom density, considering transfer of one electron per surface atom, of 241 $\mu C/cm^2$ for Pt(111),[34] 209 $\mu C/cm^2$ for Pt(100),[34] and 147 $\mu C/cm^2$ for Pt(110).[92] The reverse scan in the cyclic voltammogram is given by $-j_{X^*}$

The Gibbs free energy of adsorption, ΔG_{X^*}, is calculated as described in eq 14. For the adsorption reactions which are explicitly coverage dependent, an approximation to the configurational entropy[34] is added to the Gibbs free energies of adsorption calculated by eq 14. The configurational entropy is defined as

$$S = k_B \ln\left(\frac{1-\theta}{\theta}\right) \quad (24)$$

A linear function is fit to a plot of ΔG_{X^*} vs θ_{X^*}, plugged into the adsorption equilibrium constant expression, eq 21, which is then solved with eqs 22 and 23 to simulate the cyclic voltammogram, in terms of j_{X^*} vs U.

Cyclic voltammograms are simulated for both coverage-dependent adsorption and electrochemical "phase-change" reactions, which have been simplified here to be coverage independent. While the free energy change for the phase change reaction does depend on the coverage of each species before and after the phase change, only one coverage of each species is examined. In the electrochemical phase change, hydrogen is desorbed (adsorbed) and hydroxide adsorbed (desorbed). Phase change reactions are simulated for competitive hydrogen and hydroxide adsorption on Pt(100) and Pt(110). For both facets, the starting hydrogen coverage is 1 ML, and the final hydroxide coverage is given by the respective minimum energy coadsorbed hydroxide and water structure (1/3 ML OH* on Pt(100) and 1/2 ML OH* on Pt(110)). This phase change reaction is given in reaction 25.

$$(H_2O)_nxH^* \rightarrow yOH^*(n-y)H_2O^* + (x+y)e^- + (x+y)H^+_{aq} \quad (25)$$

DOI: 10.1021/acs.jpcc.5b10979
J. Phys. Chem. C XXXX, XXX, XXX−XXX

$$\Delta G_{H^*\rightarrow OH^*H_2O^*}(U_{NHE}) = G_{yOH^*(n-y)H_2O^*} + (x+y)eU_{NHE} - G_{(H_2O)_nxH^*} - (x+y)G_{H^+_{aq}} \quad (26)$$

The same procedure is used to calculate the Gibbs free energy change for the reaction as is used in eqs 14 and 15, yielding eq 26. The effect of coadsorbed potassium on the phase change reaction is also considered, using eq 26, where now the free energy of the adsorbed hydrogen and adsorbed hydroxide states also contains coadsorbed potassium (at the same coverage in both states). Dipole moment changes were neglected here, as they were small in both cases, giving a change in reaction free energy of less than 0.005 eV when included.

RESULTS

Hydrogen Adsorption. The adsorption of hydrogen onto Pt(111), Pt(100), and Pt(110) as a function of coverage was modeled using DFT. Adsorption favorability is given by the calculated equilibrium adsorption potential in Figure 1. Since hydrogen adsorption is a reduction process, adsorption is favorable (the ΔG becomes negative) at any potential more negative of the equilibrium adsorption potential.

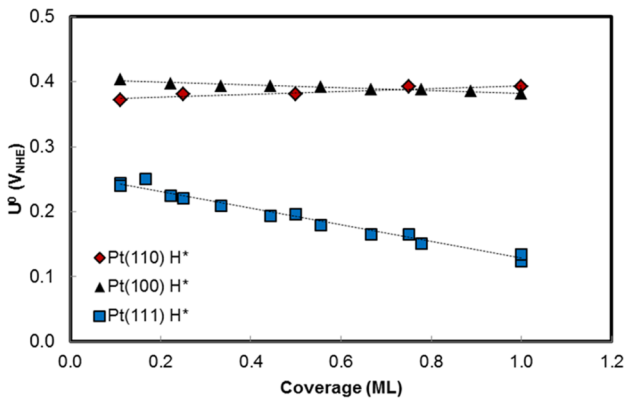

Figure 1. Equilibrium adsorption potentials (U^0, V_{NHE}) for the adsorption of hydrogen from a pH = 0 solution as a function of coverage (ML) onto Pt(111) (blue square), Pt(100) (black triangle), and Pt(110) (red diamond). Dotted lines are linear regressions of the plotted data.

The adsorption of hydrogen on Pt(111) is significantly dependent on coverage, relative to the other low index facets, with adsorption becoming less favorable as the coverage is increased. This is a well-known phenomenon that has been observed both experimentally by cyclic voltammetry[14,29,92] and temperature-programmed desorption (TPD) in ultrahigh vacuum (UHV) experiments[93−95] and computationally.[34,95,96] This strong coverage dependence has been ascribed to significant repulsion between the hydrogen adsorbates.[14,92−94] The calculated slope of adsorption potential vs coverage compares well with the slope of the adsorption energy vs coverage calculated by Karlberg et al. with DFT (0.15[34] vs 0.128 eV/ML).[34] The slope calculated here also compares well to that derived from cyclic voltammetric experiments in $HClO_4$ via rigorous thermodynamic analysis by Garcia-Araez et al. and Gómez et al. (0.303,[29] 0.295,[15] 0.285,[14] vs 0.267 eV/ML (our slope with configurational entropy included)). The negative of the intercept, which gives the ΔG of adsorption when $\theta_H{}^* = 0$, matches experiment as well (−0.285 to −0.291 eV[14,15,29] vs −0.256 eV).

The adsorption of hydrogen onto Pt(100) and Pt(110) is significantly more favorable than on Pt(111), which is to be expected given their lower surface atom coordination. On Pt(100), the intercept at zero coverage compares well to that found by Garcia-Araez et al. (−0.386 eV[29] vs −0.404 eV), with our DFT results suggesting slightly stronger binding than found experimentally. The calculated slope of adsorption potential vs coverage also differs slightly (0.073 eV/ML[29] vs 0.021, or 0.160 eV/ML, with configurational entropy), with our DFT calculations suggesting a slightly stronger repulsion when configurational entropy is included than what is measured experimentally in an electrochemical environment. Our DFT results for H adsorption on Pt(100) match prior DFT work well; our slope is similar to that found by Karlberg et al. (0.034 eV/ML[34] vs 0.021 eV/ML). The small dependence on coverage suggests only weak repulsion between adsorbed hydrogen atoms on Pt(100). The trend in hydrogen adsorption favorability between Pt(111) and Pt(100) calculated here matches TPD data from UHV experiments, with hydrogen desorbing at a higher temperature, indicating stronger binding, and with a narrower desorption peak, indicating less repulsion between adsorbates on Pt(100) and 100 steps than on Pt(111) and 111 terraces.[19−21,97] The deviation in the electrochemical environment may be due to the competitive or coadsorption of hydroxide onto the Pt(100) surface, as suggested previously,[14,17,91] but this has not been previously evaluated using DFT techniques. We examine this in the following sections.

The favorability of hydrogen adsorption on Pt(110) deviates significantly from that measured in electrochemical experiments, where hydrogen adsorption appears to be less favorable and occurs at lower potentials on Pt(110) and 110 steps than on the other low index facets.[14−17,22,29,59,92] TPD and DFT data suggest hydrogen adsorption favorability on Pt(110) (1 × 2) bridge sites, and 110 steps on Pt(553) fall intermediate to that of hydrogen adsorption on 100 steps and 111 terraces on higher-order Pt(533) and Pt(211),[19−21,98] roughly matching what our DFT results suggest but conflicting with electrochemical experimental results.

To more easily visualize the discrepancy between DFT/UHV and electrochemical experiments, cyclic voltammograms are simulated for hydrogen adsorption and are given in Figure 2.

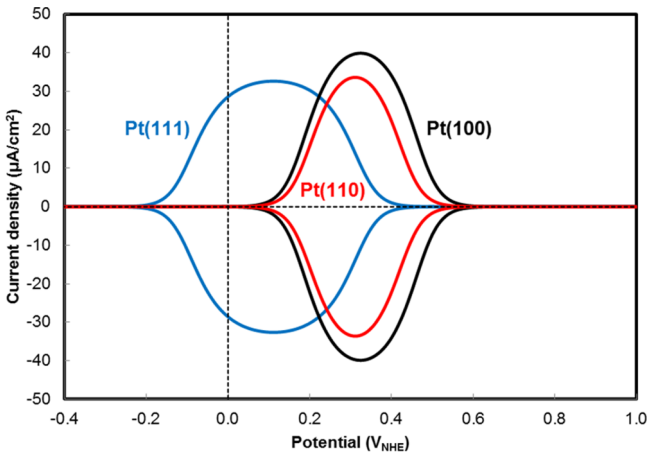

Figure 2. Simulated cyclic voltammograms for hydrogen adsorption onto a bare surface from a pH = 0 solution onto Pt(111), Pt(100), and Pt(110) electrode surfaces. Scan rate is 50 mV/s. It is assumed 1 ML of hydrogen is the maximum coverage reached on each facet.

DOI: 10.1021/acs.jpcc.5b10979
J. Phys. Chem. C XXXX, XXX, XXX−XXX

Configurational entropy contributions have been added to the data shown in Figure 1 to produce the cyclic voltammograms. They are each simulated at a scan rate of 50 mV/s, a surface site atom density of 241 $\mu C/cm^2$ for Pt(111), 209 $\mu C/cm^2$ for Pt(100), and 147 $\mu C/cm^2$ for Pt(110), and under the assumption that hydrogen adsorption reaches a maximum coverage of 1 monolayer (ML) on each of the three facets.

Following the discussion from Figure 1, the simulated cyclic voltammogram for hydrogen adsorption on Pt(111) matches experiment well, in terms of both the absolute location of the peak and its broad shape, indicating significant repulsion between adsorbed hydrogen on this surface.[14,17] The shape and location of the hydrogen adsorption peak on Pt(100) is close to what is measured experimentally,[14,17] but the simulated voltammogram peak for hydrogen adsorption on Pt(110) occurs at potentials significantly more positive than those measured experimentally,[14,17] by about 0.2 V. Both the minor deviation from experiment for the hydrogen adsorption on Pt(100) and the significant deviation for hydrogen adsorption on Pt(110) seen in Figure 2 may be due to a variety of effects, but it has been suggested previously[14,17,91,99] that hydroxide adsorption may occur near potentials where hydrogen adsorption occurs on Pt(100) and Pt(110), resulting in a coadsorption or competitive adsorption of hydrogen and hydroxide at low potentials. The effect of this competitive or coadsorption on cyclic voltammetry has not been examined previously using *ab initio* methods such as DFT and is considered in the next section.

Hydroxide and Solvated Hydroxide Adsorption. In an effort to identify the discrepancy between the simulated CV in Figure 2 and experiment for Pt(100) and Pt(110) electrode surfaces, the adsorption of hydroxide and its coadsorption with water onto Pt(111), Pt(100), and Pt(110) are considered. As has been found previously,[18,81] the presence of coadsorbed water has a significant effect on the adsorption favorability of hydroxide onto platinum. Therefore, we simulate hydroxide alone at low coverage, hydroxide with one coadsorbed water molecule at low coverage, and hydroxide with a coadsorbed water bilayer at varying coverages.

Figure 3 gives the favorable adsorption potential ranges for hydroxide adsorption, both at low coverage (1/9 ML) and in the optimal OH/H_2O coadsorbed minimum energy structures (MES). Images of these adsorbed structures are given in the Supporting Information. Coadsorbed water reduces the equilibrium adsorption potential for hydroxide on all of the low index platinum facets, as hydrogen bonds with neighboring water stabilize surface OH*. For comparison, the adsorption potential range of 1/9 ML hydrogen is shown. The well-known "double-layer" region can be seen on Pt(111) with a roughly 0.4 V window separating hydrogen adsorption from hydroxide adsorption. Experimentally, hydroxide adsorption on Pt(111) is known to begin around 0.55 V_{NHE} with a sharp peak just below 0.8 V_{NHE} in perchloric acid,[14] which compares well to the potential shown in Figure 3 when coadsorbed water is included. Fully describing hydroxide adsorption as a function of coverage requires modeling the adsorbed hydroxide−water bilayer structure, which is not explicitly known for Pt(110) and has only been recently evaluated for Pt(100). We find our results with the adsorbed water/bilayer structure are comparable to those with just one water molecule adsorbed and therefore leave a more detailed analysis of particular water structures for future work.

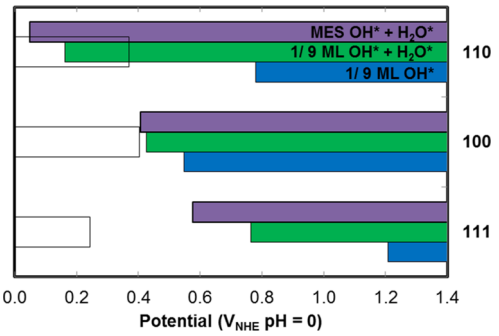

Figure 3. Favorable adsorption potentials ranges (V_{NHE}) calculated for hydrogen and hydroxide adsorption from a pH = 0 solution onto Pt(111), Pt(100), and Pt(110). Hydrogen adsorption potentials are calculated at 1/9 ML coverage. Hydroxide adsorption potentials shown in blue (bottom) are calculated at a coverage of 1/9 ML; those in green (middle) are 1/9 ML OH* and solvated by a single water molecule; and those in purple (top) are the minimum energy hydroxide and water coadsorbed structures (MES). MES for Pt(111) and Pt(100) are 1/3 ML OH* and 1/3 ML H_2O* and for Pt(110) is 1/2 ML OH* and 1/2 ML H_2O*.

Hydroxide adsorption can occur at low potentials on Pt(100) and Pt(110) within the traditional "hydrogen adsorption region", as shown by the overlapping H* and OH* potential ranges in Figure 3. Supporting assertions by Clavilier et al.,[23] van der Niet et al.,[17] Gómez et al.,[28] and Garcia-Araez et al.,[15,22,29,91] hydroxide could coadsorb or compete with hydrogen adsorption on Pt(100) and Pt(110), driving hydrogen desorption to lower potentials on these facets than what is predicted by DFT for isolated hydrogen adsorption. Relative to Pt(111), Pt(100) and Pt(110) not only bind hydrogen more strongly but also bind hydroxide (and coadsorbed water) more strongly, matching both intuition and experiment, where there is no clear hydroxide adsorption feature at high potentials in cyclic voltammograms on Pt(100) and Pt(110).

The DFT trend in hydroxide adsorption favorability with coadsorbed water across the low index platinum facets matches well with results from thermally programmed desorption (TPD) in UHV experiments. The adsorption of water on a platinum surface that has been precovered with adsorbed oxygen has been shown to produce mixed OH + H_2O layers on platinum surfaces.[89,100−102] The formation of these mixed, hydrogen-bonded adlayers drives the desorption of water to higher temperatures, indicating stronger binding relative to water adsorption on a bare surface. The temperature of the water desorption peak from TPD from an oxygen precovered surface then indicates the relative stability of the adsorbed hydroxide and water layer. The hydroxide and water adlayer is least stable on Pt(111) (200 K)[89,102] and most stable on facets containing 100 and 110 steps, including Pt(533) (270 K)[101] and Pt(553) (235 K),[100] respectively. While we match the trend between Pt(111) and stepped surfaces, we predict the opposite stability trend between 100 steps and 110 steps; this could be due to an interaction between step and terrace sites on the higher-order facets which is not captured by our single facet DFT slab models.

The overlap of the hydrogen adsorption and hydroxide adsorption regions on Pt(100) and Pt(110) is further supported by prior DFT studies which evaluated the dissociation of water on platinum steps and terraces.[18,30−32] Fajín et al. predicted the coadsorption energy of H and OH on

DOI: 10.1021/acs.jpcc.5b10979
J. Phys. Chem. C XXXX, XXX, XXX−XXX

Pt(111), Pt(100), and Pt(110) and show that the energy to coadsorb both species from water molecule dissociation, which should be proportional to the width of the "double-layer" region separating the adsorption of both species in a CV, is positive on Pt(111) but negative on Pt(100) and Pt(110).[31,103] This suggests that the hydrogen adsorption region and hydroxide adsorption region do not overlap on Pt(111) but do overlap on Pt(100) and Pt(110).[31] A similar conclusion is reached examining the results of Peköz et al.[30] While Fajín et al. show the same trend in stability between hydroxide adsorbed on Pt(100) and Pt(110) as we do here (Figure 3), they do not consider the effects of coadsorbed water on the binding strength of hydroxide.[31]

Cyclic voltammograms were again simulated, but now including the possibility of competitive adsorption of hydrogen and solvated hydroxide on Pt(100) and Pt(110) (Figure 4). To

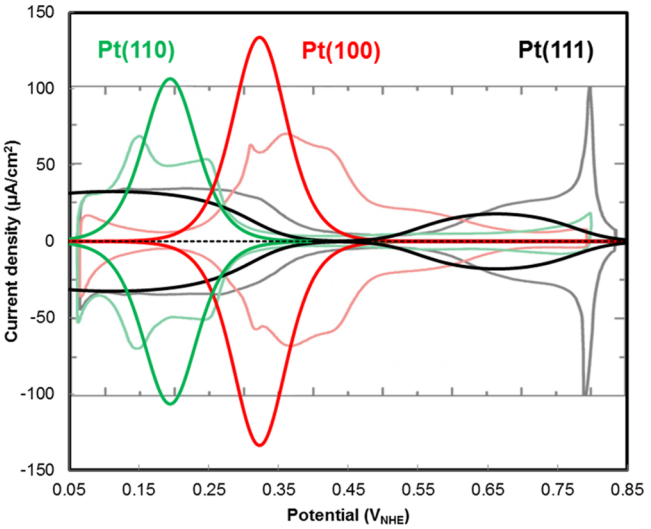

Figure 4. Simulated cyclic voltammograms for hydrogen and hydroxide adsorption from a pH = 0 solution onto Pt(111), Pt(100), and Pt(110) electrode surfaces. Adsorption/desorption on Pt(100) and Pt(110) is taken to occur through a H/OH surface phase change process. Scan rate is 50 mV/s. One ML of hydrogen is the assumed maximum coverage reached on each facet. The hydroxide coverage is that of the minimum energy OH* + H_2O* structure and is 1/3 ML OH* and 1/3 ML H_2O* on Pt(111) and Pt(100) and is 1/2 ML OH* and 1/2 ML H_2O* on Pt(110). The background data (faint lines) are experimentally measured cyclic voltammograms in 0.1 M $HClO_4$ at 50 mV/s on single-crystal electrodes adapted from N. Garcia-Araez.[29] The texture seen in the experimentally measured cyclic voltammograms would be better captured if the coverage dependence of hydrogen adsorption, hydroxide adsorption, and hydrogen and hydroxide coadsorption was considered.

model competitive adsorption of hydrogen and hydroxide, we considered the possibility of a phase change, that is, that the surface went from being predominately covered by hydrogen to predominately covered by hydroxide and water (and the reverse for the backward scan in the cyclic voltammogram). Our DFT results suggest hydrogen and hydroxide adsorption would be less competitive on Pt(100), which is supported by cyclic voltammograms on Pt(100) single crystals, where the low potential peak can be fairly well deconvoluted to show coadsorption when the hydrogen coverage is low.[14,91] However, the H/OH phase change reaction represents a computationally more tractable modeling choice. It allows for consistent treatment of near surface water between the Pt(100) and Pt(110) facets, especially in the presence of coadsorbed potassium, which has a strong interaction with water, as considered in a later section. Cyclic voltammograms for the coadsorption of hydrogen and hydroxide on Pt(100), assuming no interaction between adsorbed hydrogen and hydroxide, are provided in the Supporting Information for comparison.

Figure 4 illustrates the cyclic voltammograms for the phase change reaction for hydrogen desorption and hydroxide + water adsorption on Pt(100) and Pt(110) (and the reverse reaction for the backward scan in the cyclic voltammogram). The competitive adsorption of hydroxide shifts the low potential peak on Pt(110) to lower potentials, by ∼0.12 V, and the peak on Pt(100) by ∼0.01 V, relative to isolated hydrogen adsorption/desorption (relative to Figure 2). The order of the low potential peaks for adsorption on Pt(100) and Pt(110) now matches that given by experimentally measured CVs in 0.1 M perchloric acid. The peak corresponding to adsorption on Pt(110) is ∼0.13 V below the Pt(100) peak (∼0.15 V,[4] 0.13 V[17]). Furthermore, we also capture the absolute location of the peaks very well compared to experimental CVs in perchloric acid. We predict the peak on Pt(110) to be ∼0.07 V more positive than what is measured experimentally on (110) steps[4,17] and within the center of the broader peak measured on low index Pt(110).[14,29] We predict the peak on Pt(100) to be ∼0.05 V more positive than what is measured experimentally on (100) steps[4,17] and ∼0.05 V more negative than on low index Pt(100).[14,29] The magnitude and narrow width of these competitive adsorption peaks also match experiment much better than for isolated hydrogen adsorption.[14,17] The competitive adsorption exchange yields 1.5 electrons per surface atom for Pt(110) and 1.33 electrons per surface atom for Pt(100). The background of Figure 4 shows experimentally measured CVs on single-crystal Pt(111), Pt(110), and Pt(100) electrodes measured in 0.1 M perchloric acid, adapted from N. Garcia-Araez.[29] This lends great support to the conclusion that the low potential peaks measured in cyclic voltammetry on Pt(100), Pt(110), and higher-order facets which contain 100 and 110 steps represent the desorption (adsorption) of hydrogen and the adsorption (desorption) of hydroxide, as proposed previously by others.[14,23,28,99] The texture seen in the experimentally measured CVs may be due to the coverage dependence of hydrogen adsorption, hydroxide adsorption, and their competitive adsorption (which is neglected in the simulated CVs shown in Figure 4) on extended Pt(100) and Pt(110) surfaces,[29] as these features are absent in higher-order single-crystal CVs which contain 100 and 110 steps.[17] For comparison, Figure 4 also contains the simulated hydrogen adsorption CV for adsorption onto Pt(111) as given in Figure 2 as well as the simulated CV for hydroxide adsorption onto Pt(111), which has been presented previously by Rossmeisl et al. and whose methods we use here to describe hydroxide adsorption on Pt(111).[104] The Pt(111) CV is reasonably captured without considering H/OH exchange due to the ∼0.4 V separation between these processes.

With it established that the low potential peaks measured in cyclic voltammetry on Pt(100), Pt(110), stepped, and polycrystalline platinum are due to the co- or competitive adsorption of hydrogen and hydroxide, we can investigate the mechanism of how pH effects the location of these peaks. As the pH is increased, the electrochemical window in an aqueous solution is driven to more negative potentials on an absolute scale, making the specific adsorption of a cation in the H* potential range more favorable. We next consider the specific

DOI: 10.1021/acs.jpcc.5b10979
J. Phys. Chem. C XXXX, XXX, XXX−XXX

adsorption of a potassium cation and its effects, once specifically adsorbed, on hydrogen adsorption and hydroxide adsorption.

Potassium Cation Adsorption. Variations in pH could affect the specific adsorption of hydrogen and hydroxide/water via a few different, but related, mechanisms. Increasing pH causes a negative shift in the absolute potential at which hydrogen and hydroxide adsorb since their concentrations, and therefore their activity, change with pH. This change will not alter the H/OH adsorption potentials on a relative hydrogen electrode scale. The change in absolute potential could alter the interfacial water structure at the electrode surface, change the electric field or ion distribution near the electrode surface, and increase the favorability to adsorb cations other than protons that are present in the electrolyte solution.

The absolute potential affects the structure and dynamics of water near the electrode surface;[105−107] however, the presence of water near the electrode surface has a negligible effect on hydrogen adsorption.[34,81] The change in electric field near the surface, beyond changing the water structure, would affect the binding of adsorbates which generate a strong surface normal dipole moment. The changes in dipole moment on the adsorption of hydrogen and hydroxide, however, are small (Table S3 in Supporting Information). This leaves the interaction with cations other than protons as an important part of the mechanism for how increasing pH can shift the adsorption favorability of hydrogen and hydroxide. The favorability to specifically adsorb K^+ was investigated, as well as the effects of K* on the binding of hydrogen and hydroxide.

f5 Figure 5 gives the equilibrium adsorption potentials calculated for adsorption of K^+ from a 1 M electrolyte solution to Pt(111), Pt(100), and Pt(110) as a function of K* coverage. The adsorption potentials shown in Figure 5 do not include the effects of electrolyte near the electrode surface, which would act to stabilize the partially charged K* state, which generates a relatively significant surface normal dipole moment upon adsorption. The charge on potassium, calculated by a Bader charge analysis, and the surface normal dipole moments are tabulated as a function of K* coverage for adsorption onto each of the three facets in Table S4 and S5 in the Supporting Information. Effects of surface solvation are discussed shortly.

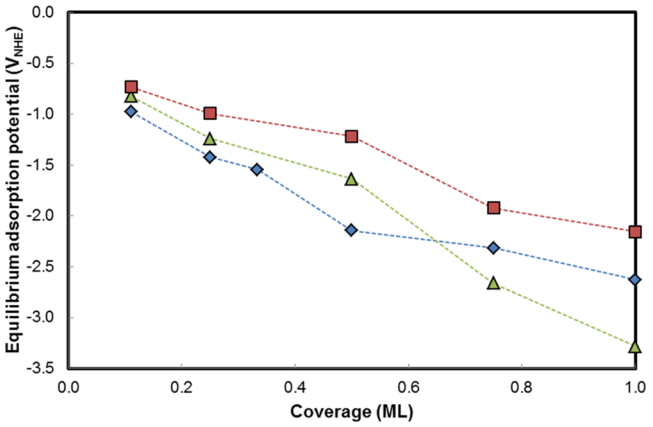

Figure 5. Equilibrium adsorption potential (V_{NHE}) calculated for K^+ adsorption from a 1 M solution onto Pt(111) (blue diamonds), Pt(100) (green triangles), and Pt(110) (red squares) as a function of potassium coverage (ML). Equilibrium adsorption potentials neglect solvation stabilization of K* at the Pt surface, which would shift K* adsorption to more positive potentials.

Adsorption of K* is favorable within the electrochemical window of water in an alkaline electrolyte (lower limit −0.826 V_{NHE} for HER/HOR at pH = 14) up to a coverage of 1/4 ML on all three of the low index facets of platinum. Therefore, we expect low coverage K* specific adsorption to be competitive with hydrogen adsorption at low potentials on Pt(111), Pt(100), and Pt(110) in an alkaline electrolyte. Solvation by water near the electrode surface would drive adsorption to higher coverages within this window. This would also make K* specific adsorption competitive with hydrogen adsorption in lower pH electrolytes. Figure 5 also shows that the adsorption of K^+ onto all three low index Pt facets is strongly coverage dependent, and as such, we would not expect the coverage of K* to exceed 1/3 ML on Pt(111) or 1/2 ML on Pt(100) and Pt(110). Given the size of the potassium cation and the small positive charge it retains on adsorption (Table S5), this strong dependence on coverage is primarily due to electrostatic repulsion at low coverages and a combination of electrostatic repulsion and steric hindrance at high coverages.

To examine the effects of electrolyte near the electrode surface on the adsorption of K^+, the favorability of K^+ adsorption at 1/9 ML on Pt(111), Pt(100), and Pt(110) was examined in the presence of one, three, and six explicit water molecules placed near the surface adsorbate and with an implicit solvation model implemented in VASP.[82] Our group previously concluded, for the Pt(111) surface, that the adsorption favorability of alkali cations is roughly converged with six explicit water molecules.[37] These adsorption potentials are plotted in Figures S6, S7, and S8 in the Supporting Information. The effect of including explicit water molecules on all of the three facets is to make adsorption more favorable by ~0.6−0.8 eV. Implicit solvation shows a similar effect. Water near the electrode surface can stabilize the charge retained on potassium after its specific adsorption, making adsorption more favorable.

Potassium cations can specifically adsorb to Pt(111), Pt(100), and Pt(110) in the H* potential region in alkaline electrolytes and could affect the adsorption of hydrogen or hydroxide. With the effects of surface solvation approximated, they may specifically adsorb at low coverage in lower pH electrolytes as well, even including in a pH = 0 electrolyte. We next examine if alkali cation specific adsorption can cause the experimentally observed shifts in the H/OH exchange potentials with pH on Pt(110) and Pt(100) by examining K/H and K/OH coadsorption.

Hydrogen and Potassium Coadsorption. f6 Figure 6 shows the calculated hydrogen adsorption potential at 1 ML coverage on Pt(111), Pt(100), and Pt(110) as a function of coadsorbed potassium coverage, from θ_{K^*} = 0 to 0.25 ML. The interaction between K* and H* is slightly repulsive at all coverages investigated on each of the three facets. This makes hydrogen adsorption less favorable, driving its equilibrium adsorption potential lower. This repulsive interaction is strongest on Pt(111) and Pt(100), but the overall magnitude of the interaction is weak, never exceeding 0.15 eV. The effect is almost negligible on Pt(110). Further examination of this interaction, including the free energy of interaction between adsorbed hydrogen and adsorbed potassium (Table S9) and the change in the charge of adsorbed hydrogen in the presence of specifically adsorbed potassium (Table S10), is given in the Supporting Information.

DOI: 10.1021/acs.jpcc.5b10979
J. Phys. Chem. C XXXX, XXX, XXX−XXX

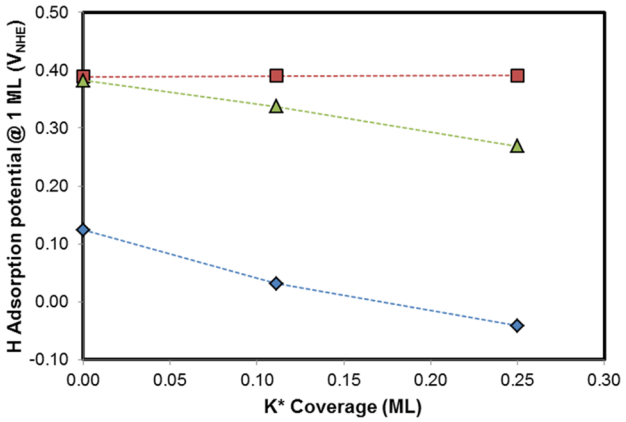

Figure 6. Equilibrium adsorption potential (V_{NHE}) calculated for adsorption of 1 ML of hydrogen from a pH = 0 solution next to specifically adsorbed potassium (K*) on Pt(111) (blue diamonds), Pt(100) (green triangles), and Pt(110) (red squares) as a function of adsorbed potassium coverage (ML).

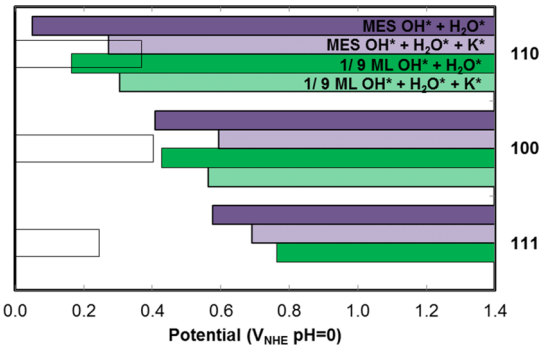

Figure 7. Equilibrium adsorption potentials (V_{NHE}) calculated for hydrogen and hydroxide adsorption from a pH = 0 solution onto Pt(111), Pt(100), and Pt(110). Hydrogen adsorption potentials are calculated at 1/9 ML coverage (left-hand axis). Hydroxide adsorption potentials in purple (top bar) and green (3rd from top bar) are the same as in Figure 3. Hydroxide adsorption potentials in light purple (2nd bar from top) are calculated using the minimum energy hydroxide and water structures (MES) but with coadsorbed potassium at 1/9 ML on Pt(111) and Pt(100) and at 1/4 ML on Pt(110). Hydroxide adsorption potentials given by the light green bar (bottom) are calculated with 1/9 ML OH*, 1/9 ML H_2O*, and 1/9 ML K*. The equilibrium adsorption potential is given by the right most edge of the bar (hydrogen adsorption, white bar, left-hand axis) or by the left most edge (hydroxide adsorption).

Given that the interaction between adsorbed hydrogen and adsorbed potassium is almost negligible on Pt(110) and that the interaction is repulsive on Pt(100), this interaction cannot explain the experimentally measured shift of the Pt(100) and Pt(110) low potential CV peaks to higher potential with increasing pH. The presence of coadsorbed potassium, favored by higher pH, weakens hydrogen binding, whereas experimentally, the adsorption peak shifts to higher potentials, suggesting stronger hydrogen binding as pH is increased.[4,17]

This leads us to consider the effect of specifically adsorbed potassium on hydroxide adsorption to explain these experimentally measured effects, as we showed that these low potential peaks on Pt(110) and Pt(100) are actually due to the competitive adsorption of hydrogen and hydroxide (Figure 4).

Hydroxide–Water–Potassium Coadsorption. We established in the section entitled "Hydrogen and hydroxide and water co-adsorption" that the low potential adsorption peaks measured in cyclic voltammetry on Pt(100) and Pt(110)[4,14,15,17] are the competitive or coadsorption of hydrogen and hydroxide (Figure 4). Experimentally, these peaks shift to higher potentials with increasing pH.[4,17] The previous section showed that this shift cannot be explained by the interaction of specifically adsorbed potassium and specifically adsorbed hydrogen (Figure 6). We therefore consider that specifically adsorbed potassium may affect the adsorption of hydroxide and water. Given that potassium tends to retain some of its charge on adsorption (Tables S4 and S5), it seems logical that the interaction between K* and OH* + H_2O* could be significant, at least more so than the interaction with nonpolar H*.

To examine the interaction between K* and OH* + H_2O*, the hydroxide adsorption potential was calculated for K* and OH* coadsorption in three structures: (1) OH* at 1/9 ML next to 1/9 ML K* on Pt(111), Pt(100), and Pt(110), (2) the adsorption of OH* at 1/9 ML next to 1/9 ML K* and 1/9 ML H_2O* on Pt(111), Pt(100), and Pt(110), and (3) the adsorption of OH* in the minimum energy OH + H_2O structure next to K* [at 1/9 ML K*, 1/3 ML OH*, and 1/3 ML H_2O* on Pt(111) and Pt(100), and K* at 1/4 ML, OH 1/2 ML, and H_2O 1/2 ML on Pt(110)]. The adsorption potentials calculated with water included are given in Figure 7. Without water included (K* 1/9 ML, OH* 1/9 ML), the interaction was found to be significantly attractive, counter to what was found for all of the structures that include coadsorbed water; these results are given separately in the Supporting Information (Table S11).

Specifically adsorbed K* drives the adsorption of OH* with coadsorbed H_2O* to more positive potentials, making surface hydroxide formation less stable. This effect matches the experimentally measured trend in cyclic voltammetry; as the pH is increased and potassium adsorption made more favorable, the low potential peaks on Pt(100) and Pt(110) shift to more positive potentials. There is no effect on the broad Pt(111) low potential peak because OH* adsorption occurs at potentials significantly more positive than this H* adsorption/desorption peak. To better compare with experiment, cyclic voltammograms are again simulated for the phase change reaction, but now with and without the presence of specifically adsorbed potassium.

Figure 8 plots the cyclic voltammogram simulated at 50 mV/s and 300 K for the phase change reactions on Pt(100) and Pt(110) in the presence of specifically adsorbed potassium. As potassium specific adsorption becomes more favorable as pH is increased, the simulated voltammograms with coadsorbed K* represent the expected CVs in an alkaline electrolyte. These CVs compare very well with those experimentally measured in 0.1 M KOH.[4,99,108,109] While we predict the competitive adsorption of hydrogen and hydroxide in an alkaline solution on Pt(110) at a slightly higher potential, 0.35 V_{RHE}, than what is measured experimentally, 0.28 V_{RHE},[4] we predict the location of the competitive adsorption peak on Pt(100) very well, 0.41 vs ~0.4 V_{RHE} measured experimentally.[4] More importantly, we capture the shift with pH very well between CVs measured in 0.1 M $HClO_4$ and 0.1 M KOH; for Pt(110) we calculate a shift of 0.155 V_{RHE} compared to ~0.15 V_{RHE};[4] for Pt(100) our calculated shift of 0.09 is a little less than what is measured experimentally, ~0.13 V_{RHE}.[4] The presence of specifically adsorbed K* at high pH weakens the binding of solvated

DOI: 10.1021/acs.jpcc.5b10979
J. Phys. Chem. C XXXX, XXX, XXX–XXX

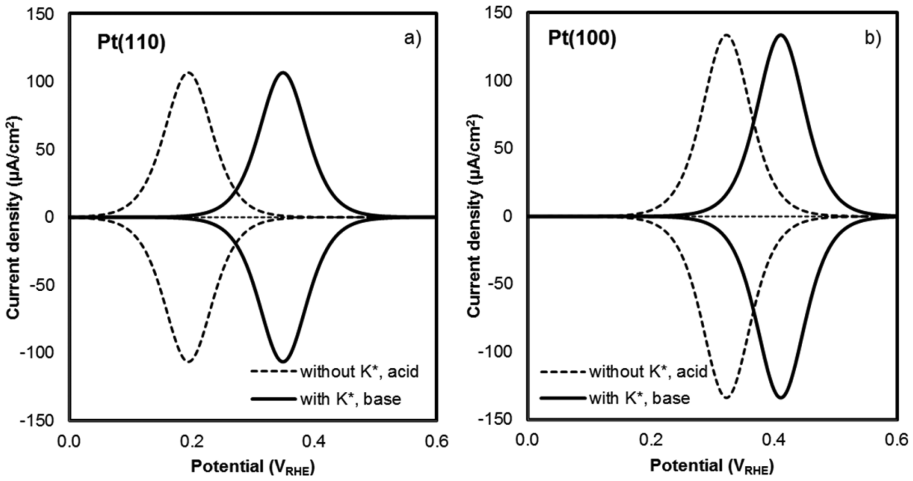

Figure 8. Simulated cyclic voltammograms for hydrogen and hydroxide adsorption from a pH = 0 solution via a phase change reaction onto (a) Pt(110) and (b) Pt(100) electrode surfaces in the absence (dotted lines) and presence (solid lines) of specifically adsorbed potassium. Scan rate is 50 mV/s. The hydroxide coverage is of the minimum energy OH* + H_2O* structure and is 1/3 ML OH* and 1/3 ML H_2O* on Pt(100) and is 1/2 ML OH* and 1/2 ML H_2O* on Pt(110). Hydrogen coverage is 1 ML on all three facets. K* coverage is 1/9 ML on Pt(100) and 1/4 ML on Pt(110). The absence of specifically adsorbed potassium represents the conditions expected in acid electrolytes, and the presence of specifically adsorbed potassium represents the conditions expected in basic electrolytes, with the coverage of K* varying with pH.

hydroxide and therefore shifts the H*/OH* replacement/phase change potential to more positive values.

Figure 9 plots the formation potential for surface hydroxide as a function of potassium coverage, illustrating that as the K*

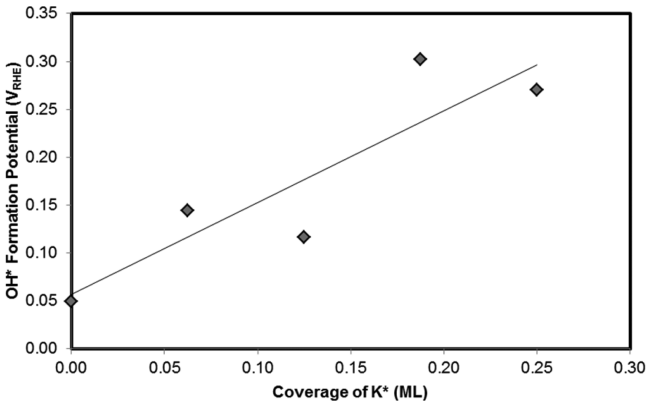

Figure 9. Equilibrium formation potential for hydroxide in its minimum energy structure with coadsorbed water from adsorbed water on Pt(110) for formation next to specifically adsorbed potassium as a function of potassium coverage (ML). The solid line is a linear regression, intended only as a guide to the general trend.

coverage is increased the favorability to adsorb hydroxide progressively decreases. This results in the hydroxide equilibrium adsorption potential rising to more positive potentials at higher K* coverages. This trend matches very well with the results by Sheng et al.[4] and van der Niet et al.,[17] which show that as the pH increases the "hydrogen binding energy", which we have now concluded is actually a H*/OH* replacement reaction energy, increases as well, with a slope of about −10 mV_{RHE}/pH unit. As the pH of the electrolyte is increased, the favorability to adsorb potassium increases, increasing the potassium coverage on the surface, making hydroxide adsorption less favorable, causing the 110 and 100 CV peaks measured at low potentials to shift to more positive potentials. It is difficult to compare our slope of hydroxide adsorption potential versus K* coverage directly to experiment, as that requires a precise evaluation of K* adsorption energy vs coverage which is too dependent on the imprecision of using static H_2O molecules to solvate K* in DFT calculations.

The conclusion that K* coadsorption weakens hydroxide adsorption in the solvated environment is counterintuitive, given the expected attraction between K* and OH*. To better understand why K* reduces the favorability to form OH*H_2O*, the surface Pt−O bond lengths, the OH*H_2O* hydrogen bond lengths, and the charge on molecular OH* and H_2O* are evaluated as a function of potassium coverage for adsorption onto the Pt(110) surface. As the potassium coverage is increased, the Pt−O bond length in the 1/2 ML OH* 1/2 ML H_2O* structure increases significantly, as given in Figure 10. This is consistent with the weakening of the Pt−O bond,

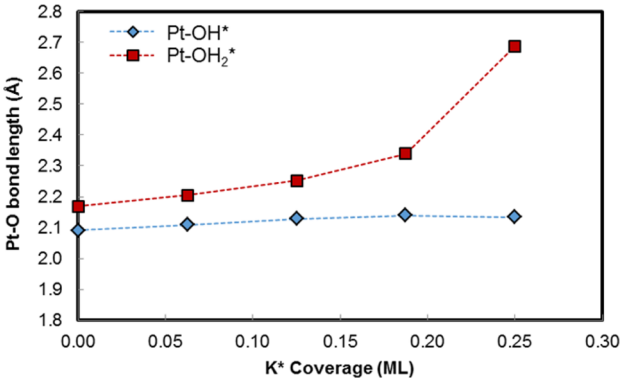

Figure 10. Pt−O bond length (Å) for adsorbed hydroxide and adsorbed water as a function of K* coverage (ML).

for oxygen in both adsorbed hydroxide and adsorbed water, as the potassium coverage is increased. This weakening contributes to the decrease in favorability to adsorb hydroxide as the potassium coverage is increased.

A more complex interaction is seen in Figure 11, which plots the OH*−H_2O* (with hydroxide as the hydrogen bond donor) hydrogen bond length and the H_2O*−OH* (with hydroxide as

DOI: 10.1021/acs.jpcc.5b10979
J. Phys. Chem. C XXXX, XXX, XXX−XXX

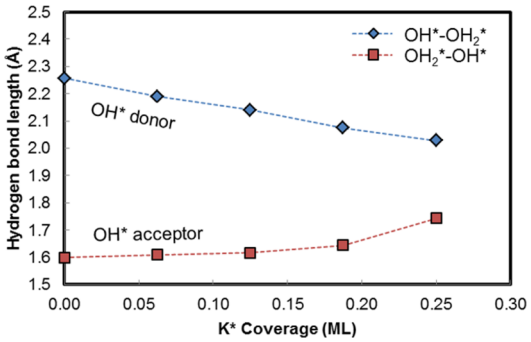

Figure 11. Hydrogen bond length (Å) between adsorbed hydroxide and adsorbed water with hydroxide as the hydrogen bond donor and as the hydrogen bond acceptor as a function of K* coverage (ML).

the hydrogen bond acceptor) hydrogen bond length as a function of potassium coverage. The "hydroxide as donor" hydrogen bond length between adsorbed hydroxide and adsorbed water decreases with increasing potassium coverage, while the hydrogen bond length with hydroxide as the acceptor increases with increasing potassium coverage. The magnitude of the change with potassium coverage is larger for hydroxide as the donor, given by the larger slope in Figure 11. As the potassium coverage is increased, bonding to the surface through oxygen seems to weaken, while hydrogen bonding between adsorbed hydroxide and adsorbed water strengthens, with the net effect of the structure becoming less stable, as indicated by the more positive hydroxide adsorption potentials with increasing potassium coverage.

Finally, the charge on the adsorbed OH* and H_2O* molecules can be evaluated as a function of K* coverage on Pt(110). Figure 12 shows the charge on adsorbed OH* and the

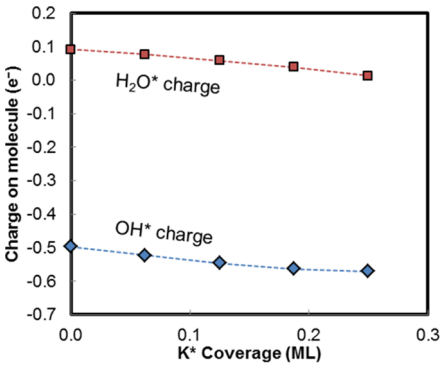

Figure 12. Charge on adsorbed hydroxide and adsorbed water molecules as a function of K* coverage on Pt(110).

charge on H_2O*, calculated via a Bader charge analysis,[71−73] vs K* coverage. As the coverage of K* is increased, both OH* and H_2O* take on more negative charge. This is expected as K* retains some positive charge on adsorption, allowing for a stabilization of more negative charge above the surface as the coverage of K* is increased.

Though the bond lengths and change in charges show a complex set of interactions, the presence of increasing amounts of K* on the Pt(110) surface drives solvated $OH_{(aq)}^-$ adsorption to be less favorable. Increasing coverage of K* produces a greater negative charge, primarily on the oxygen of OH*, lengthens the Pt−O bond to both OH* and H_2O*, and causes a restructuring of the OH* H_2O* hydrogen bonding network.

While the absolute potentials calculated here do depend on the particular coadsorbed hydroxide and water structures that we have used, the qualitative results are consistent across the multiple structures and the Pt(110) and (100) surfaces considered. Hydroxide adsorption occurs well into the hydrogen adsorption region on Pt(100) and Pt(110), and the presence of specifically adsorbed potassium weakens hydroxide binding, as supported by the calculations with one coadsorbed water molecule at a low hydroxide coverage (Figure 7). Nonspecifically adsorbed K^+ ions in the surface region may cause similar effects, though we have not examined this with DFT as our calculations indicate specific adsorption of potassium will occur.

CONCLUSIONS

The presence of reactant and spectator ions, atoms, and molecules near or adsorbed onto the electrode surface can have a complex effect on the rates and mechanisms of electrocatalytic reactions. Density functional theory was used to show that the sharp, low potential peaks in current measured experimentally by cyclic voltammetry on Pt(100), Pt(110), and higher-order stepped and polycrystalline platinum are the coadsorption or competitive adsorption of hydrogen and hydroxide. The experimentally measured variation of these peak positions with pH is due to specifically adsorbed alkali metal cations. The presence of specifically adsorbed potassium does not significantly impact H* adsorption but weakens the binding of hydroxide on the electrode surface. Less stable OH* drives the Pt(110) and (100) peaks to higher potentials on a relative hydrogen electrode scale as the pH is increased, as observed experimentally. These conclusions could have a significant impact on the electrocatalytic properties of platinum electrodes, especially for reactions which involve specifically adsorbed hydroxide. This DFT work lends significant support to the idea that hydroxide can be present on 100, 110, and stepped platinum surfaces at much lower potentials than on Pt(111). This work also illustrates the importance of alkali cation specific adsorption in effecting the adsorption of hydroxide. The shift in favorability of hydroxide adsorption with pH, which we show is due to the presence of specifically adsorbed potassium, correlates with a 2 orders of magnitude change in the rate of hydrogen oxidation/evolution[4] from acid to basic electrolytes. Understanding alkali cation effects on adsorbed reaction intermediates is therefore technologically significant.

ASSOCIATED CONTENT

Supporting Information

The Supporting Information is available free of charge on the ACS Publications website at DOI: 10.1021/acs.jpcc.5b10979.

Figures for all of the minimum energy water and hydroxide structures as well as potassium hydrogen interaction energies, potassium charges, dipole moments, and adsorption potentials (PDF)

AUTHOR INFORMATION

Corresponding Author

*E-mail: mjanik@psu.edu.

DOI: 10.1021/acs.jpcc.5b10979
J. Phys. Chem. C XXXX, XXX, XXX−XXX

Author Contributions

The manuscript was written through contributions of all authors. All authors have given approval to the final version of the manuscript.

Notes

The authors declare no competing financial interest.

■ ACKNOWLEDGMENTS

The authors gratefully acknowledge support from the National Science Foundation DMREF Grant #1436206. I.T. McCrum acknowledges support from The Pennsylvania State University Diefenderfer Graduate Fellowship and NSF NRT #1449785.

■ REFERENCES

(1) Trasatti, S. Work Function, Electronegativity, and Electrochemical Behaviour of Metals: III. Electrolytic Hydrogen Evolution in Acid Solutions. *J. Electroanal. Chem. Interfacial Electrochem.* **1972**, *39*, 163−184.

(2) Skúlason, E.; Tripkovic, V.; Björketun, M. E.; Gudmundsdóttir, S.; Karlberg, G.; Rossmeisl, J.; Bligaard, T.; Jónsson, H.; Nørskov, J. K. Modeling the Electrochemical Hydrogen Oxidation and Evolution Reactions on the Basis of Density Functional Theory Calculations. *J. Phys. Chem. C* **2010**, *114*, 18182−18197.

(3) Strmcnik, D.; Uchimura, M.; Wang, C.; Subbaraman, R.; Danilovic, N.; van der Vliet, D.; Paulikas, A. P.; Stamenkovic, V. R.; Markovic, N. M. Improving the Hydrogen Oxidation Reaction Rate by Promotion of Hydroxyl Adsorption. *Nat. Chem.* **2013**, *5*, 300−306.

(4) Sheng, W.; Zhuang, Z.; Gao, M.; Zheng, J.; Chen, J. G.; Yan, Y. Correlating Hydrogen Oxidation and Evolution Activity on Platinum at Different pH with Measured Hydrogen Binding Energy. *Nat. Commun.* **2015**, *6*, 5848.

(5) Antoine, O.; Bultel, Y.; Durand, R. Oxygen Reduction Reaction Kinetics and Mechanism on Platinum Nanoparticles inside Nafion®. *J. Electroanal. Chem.* **2001**, *499*, 85−94.

(6) Tripković, V.; Skúlason, E.; Siahrostami, S.; Nørskov, J. K.; Rossmeisl, J. The Oxygen Reduction Reaction Mechanism on Pt(1 1 1) from Density Functional Theory Calculations. *Electrochim. Acta* **2010**, *55*, 7975−7981.

(7) Wang, J. X.; Markovic, N. M.; Adzic, R. R. Kinetic Analysis of Oxygen Reduction on Pt(111) in Acid Solutions: Intrinsic Kinetic Parameters and Anion Adsorption Effects. *J. Phys. Chem. B* **2004**, *108*, 4127−4133.

(8) Gilman, S. The Mechanism of Electrochemical Oxidation of Carbon Monoxide and Methanol on Platinum. II. The "Reactant-Pair" Mechanism for Electrochemical Oxidation of Carbon Monoxide and Methanol. *J. Phys. Chem.* **1964**, *68*, 70−80.

(9) Garcia, G.; Koper, M. T. M. Mechanism of Electro-Oxidation of Carbon Monoxide on Stepped Platinum Electrodes in Alkaline Media: A Chronoamperometric and Kinetic Modeling Study. *Phys. Chem. Chem. Phys.* **2009**, *11*, 11437−11446.

(10) Urchaga, P.; Baranton, S.; Coutanceau, C.; Jerkiewicz, G. Evidence of an Eley−Rideal Mechanism in the Stripping of a Saturation Layer of Chemisorbed CO on Platinum Nanoparticles. *Langmuir* **2012**, *28*, 13094−13104.

(11) Gómez-Marín, A. M.; Hernández-Ortíz, J. P. Mean Field Approximation of Langmuir−Hinshelwood CO−Surface Reactions Considering Lateral Interactions. *J. Phys. Chem. C* **2013**, *117*, 15716−15727.

(12) Cao, D.; Lu, G. Q.; Wieckowski, A.; Wasileski, S. A.; Neurock, M. Mechanisms of Methanol Decomposition on Platinum: A Combined Experimental and Ab Initio Approach. *J. Phys. Chem. B* **2005**, *109*, 11622−11633.

(13) Gisbert, R.; García, G.; Koper, M. T. M. Adsorption of Phosphate Species on Poly-Oriented Pt and Pt(1 1 1) Electrodes over a Wide Range of pH. *Electrochim. Acta* **2010**, *55*, 7961−7968.

(14) Gómez, R.; Orts, J. M.; Álvarez-Ruiz, B.; Feliu, J. M. Effect of Temperature on Hydrogen Adsorption on Pt(111), Pt(110), and Pt(100) Electrodes in 0.1 M HClO4. *J. Phys. Chem. B* **2004**, *108*, 228−238.

(15) Garcia-Araez, N.; Climent, V.; Feliu, J. Potential-Dependent Water Orientation on Pt(111), Pt(100), and Pt(110), as Inferred from Laser-Pulsed Experiments. Electrostatic and Chemical Effects. *J. Phys. Chem. C* **2009**, *113*, 9290−9304.

(16) Climent, V.; Feliu, J. Thirty Years of Platinum Single Crystal Electrochemistry. *J. Solid State Electrochem.* **2011**, *15*, 1297−1315.

(17) van der Niet, M. J. T. C.; Garcia-Araez, N.; Hernández, J.; Feliu, J. M.; Koper, M. T. M. Water Dissociation on Well-Defined Platinum Surfaces: The Electrochemical Perspective. *Catal. Today* **2013**, *202*, 105−113.

(18) Jinnouchi, R.; Nagoya, A.; Kodama, K.; Morimoto, Y. Solvation Effects on OH Adsorbates on Stepped Pt Surfaces. *J. Phys. Chem. C* **2015**, *119*, 16743−16753.

(19) Badan, C.; Koper, M. T. M.; Juurlink, L. B. F. How Well Does Pt(211) Represent Pt[N(111) × (100)] Surfaces in Adsorption/Desorption? *J. Phys. Chem. C* **2015**, *119*, 13551−13560.

(20) van der Niet, M. J. T. C.; den Dunnen, A.; Juurlink, L. B. F.; Koper, M. T. M. The Influence of Step Geometry on the Desorption Characteristics of O2, D2, and H2O from Stepped Pt Surfaces. *J. Chem. Phys.* **2010**, *132*, 174705.

(21) Lu, K. E.; Rye, R. R. Flash Desorption and Equilibration of H2 and D2 on Single Crystal Surfaces of Platinum. *Surf. Sci.* **1974**, *45*, 677−695.

(22) Garcia-Araez, N.; Climent, V.; Feliu, J. M. Analysis of Temperature Effects on Hydrogen and OH Adsorption on Pt(111), Pt(100) and Pt(110) by Means of Gibbs Thermodynamics. *J. Electroanal. Chem.* **2010**, *649*, 69−82.

(23) Clavilier, J.; Albalat, R.; Gomez, R.; Orts, J. M.; Feliu, J. M.; Aldaz, A. Study of the Charge Displacement at Constant Potential During CO Adsorption on Pt(110) and Pt(111) Electrodes in Contact with a Perchloric Acid Solution. *J. Electroanal. Chem.* **1992**, *330*, 489−497.

(24) Climent, V.; Gómez, R.; Feliu, J. M. Effect of Increasing Amount of Steps on the Potential of Zero Total Charge of Pt(111) Electrodes. *Electrochim. Acta* **1999**, *45*, 629−637.

(25) Climent, V.; Attard, G. A.; Feliu, J. M. Potential of Zero Charge of Platinum Stepped Surfaces: A Combined Approach of CO Charge Displacement and N2O Reduction. *J. Electroanal. Chem.* **2002**, *532*, 67−74.

(26) Domke, K.; Herrero, E.; Rodes, A.; Feliu, J. M. Determination of the Potentials of Zero Total Charge of Pt(100) Stepped Surfaces in the [01$\bar{1}$] Zone. Effect of the Step Density and Anion Adsorption. *J. Electroanal. Chem.* **2003**, *552*, 115−128.

(27) Attard, G. A.; Hazzazi, O.; Wells, P. B.; Climent, V.; Herrero, E.; Feliu, J. M. On the Global and Local Values of the Potential of Zero Total Charge at Well-Defined Platinum Surfaces: Stepped and Adatom Modified Surfaces. *J. Electroanal. Chem.* **2004**, *568*, 329−342.

(28) Gómez, R.; Climent, V.; Feliu, J. M.; Weaver, M. J. Dependence of the Potential of Zero Charge of Stepped Platinum (111) Electrodes on the Oriented Step-Edge Density: Electrochemical Implications and Comparison with Work Function Behavior. *J. Phys. Chem. B* **2000**, *104*, 597−605.

(29) Garcia-Araez, N. Enthalpic and Entropic Effects on Hydrogen and OH Adsorption on Pt(111), Pt(100), and Pt(110) Electrodes as Evaluated by Gibbs Thermodynamics. *J. Phys. Chem. C* **2011**, *115*, 501−510.

(30) Peköz, R.; Wörner, S.; Ghiringhelli, L. M.; Donadio, D. Trends in the Adsorption and Dissociation of Water Clusters on Flat and Stepped Metallic Surfaces. *J. Phys. Chem. C* **2014**, *118*, 29990−29998.

(31) Fajín, J. L. C.; D. S. Cordeiro, M. N.; Gomes, J. R. B. Density Functional Theory Study of the Water Dissociation on Platinum Surfaces: General Trends. *J. Phys. Chem. A* **2014**, *118*, 5832−5840.

(32) Donadio, D.; Ghiringhelli, L. M.; Delle Site, L. Autocatalytic and Cooperatively Stabilized Dissociation of Water on a Stepped Platinum Surface. *J. Am. Chem. Soc.* **2012**, *134*, 19217−19222.

(33) Kolb, M. J.; Calle-Vallejo, F.; Juurlink, L. B. F.; Koper, M. T. M. Density Functional Theory Study of Adsorption of H2O, H, O, and

DOI: 10.1021/acs.jpcc.5b10979
J. Phys. Chem. C XXXX, XXX, XXX−XXX

OH on Stepped Platinum Surfaces. *J. Chem. Phys.* **2014**, *140*, 134708-1−134708-6.
(34) Karlberg, G. S.; Jaramillo, T. F.; Skúlason, E.; Rossmeisl, J.; Bligaard, T.; Nørskov, J. K. Cyclic Voltammograms for H on Pt(111) and Pt(100) from First Principles. *Phys. Rev. Lett.* **2007**, *99*, 126101.
(35) Sheng, W.; Gasteiger, H. A.; Shao-Horn, Y. Hydrogen Oxidation and Evolution Reaction Kinetics on Platinum: Acid Vs Alkaline Electrolytes. *J. Electrochem. Soc.* **2010**, *157*, B1529−B1536.
(36) Neyerlin, K. C.; Gu, W.; Jorne, J.; Gasteiger, H. A. Study of the Exchange Current Density for the Hydrogen Oxidation and Evolution Reactions. *J. Electrochem. Soc.* **2007**, *154*, B631−B635.
(37) Mills, J. N.; McCrum, I. T.; Janik, M. J. Alkali Cation Specific Adsorption onto FCC(111) Transition Metal Electrodes. *Phys. Chem. Chem. Phys.* **2014**, *16*, 13699−13707.
(38) Matanovic, I.; Atanassov, P.; Garzon, F.; Henson, N. J. Density Functional Theory Study of the Alkali Metal Cation Adsorption on Pt(111), Pt(100), and Pt(110) Surfaces. *ECS Trans.* **2014**, *61*, 47−53.
(39) Kazarinov, V. E.; Petry, O. A. Adsorption of Cesium and Sodium Cations on a Platinum Electrode. *J. Electroanal. Chem. Interfacial Electrochem.* **1970**, *27*, A1−A2.
(40) Garcia-Araez, N.; Climent, V.; Rodriguez, P.; Feliu, J. M. Thermodynamic Evidence for K+-SO42- Ion Pair Formation on Pt(111). New Insight into Cation Specific Adsorption. *Phys. Chem. Chem. Phys.* **2010**, *12*, 12146−12152.
(41) Garcia-Araez, N.; Climent, V.; Rodriguez, P.; Feliu, J. M. Elucidation of the Chemical Nature of Adsorbed Species for Pt(111) in H2SO4 Solutions by Thermodynamic Analysis. *Langmuir* **2010**, *26*, 12408−12417.
(42) García, N.; Climent, V.; Orts, J. M.; Feliu, J. M.; Aldaz, A. Effect of pH and Alkaline Metal Cations on the Voltammetry of Pt(111) Single Crystal Electrodes in Sulfuric Acid Solution. *ChemPhysChem* **2004**, *5*, 1221−1227.
(43) Climent, V.; García-Araez, N.; Feliu, J. M. Influence of Alkali Cations on the Infrared Spectra of Adsorbed (Bi)Sulphate on Pt(1 1 1) Electrodes. *Electrochem. Commun.* **2006**, *8*, 1577−1582.
(44) Rosasco, S. D.; Stickney, J. L.; Salaita, G. N.; Frank, D. G.; Katekaru, J. Y.; Schardt, B. C.; Soriaga, M. P.; Stern, D. A.; Hubbard, A. T. Cation Competition in the Electrical Double-Layer at a Well-Defined Electrode Surface Li+, Na+, K+, Cs+, H+, Mg2+, Ca2+, Ba2+, La3+, Tetramethylammonium, Choline and Acetylcholine Cations at Pt(111) Surfaces Containing an Ordered Layer of Cyanide. *J. Electroanal. Chem. Interfacial Electrochem.* **1985**, *188*, 95−104.
(45) Horányi, G.; Rizmayer, E. M. Radiotracer Study of the Adsorption of CN− Ions and Simultaneous Adsorption of Ca2+ and CN− Ions at a Platinized Platinum Electrode in Alkaline Medium. *J. Electroanal. Chem. Interfacial Electrochem.* **1986**, *215*, 369−376.
(46) Escudero-Escribano, M.; Zoloff Michoff, M. E.; Leiva, E. P. M.; Marković, N. M.; Gutiérrez, C.; Cuesta, Á. Quantitative Study of Non-Covalent Interactions at the Electrode−Electrolyte Interface Using Cyanide-Modified Pt(111) Electrodes. *ChemPhysChem* **2011**, *12*, 2230−2234.
(47) Escudero-Escribano, M.; Soldano, G. J.; Quaino, P.; Zoloff Michoff, M. E.; Leiva, E. P. M.; Schmickler, W.; Cuesta, Á. Cyanide-Modified Pt(1 1 1): Structure, Stability and Hydrogen Adsorption. *Electrochim. Acta* **2012**, *82*, 524−533.
(48) Kim, Y.-G.; Yau, S.-L.; Itaya, K. Direct Observation of Complexation of Alkali Cations on Cyanide-Modified Pt(111) by Scanning Tunneling Microscopy. *J. Am. Chem. Soc.* **1996**, *118*, 393−400.
(49) Berkes, B. B.; Székely, A.; Inzelt, G. Effect of Cs+ Ions on the Electrochemical Nanogravimetric Response of Platinum Electrode in Acid Media. *Electrochem. Commun.* **2010**, *12*, 1095−1098.
(50) Berkes, B. B.; Inzelt, G.; Schuhmann, W.; Bondarenko, A. S. Influence of Cs+ and Na+ on Specific Adsorption of *OH, *O, and *H at Platinum in Acidic Sulfuric Media. *J. Phys. Chem. C* **2012**, *116*, 10995−11003.
(51) Strmcnik, D.; Kodama, K.; van der Vliet, D.; Greeley, J.; Stamenkovic, V. R.; Marković, N. M. The Role of Non-Covalent Interactions in Electrocatalytic Fuel-Cell Reactions on Platinum. *Nat. Chem.* **2009**, *1*, 466−472.
(52) Ganassin, A.; Colic, V.; Tymoczko, J.; Bandarenka, A. S.; Schuhmann, W. Non-Covalent Interactions in Water Electrolysis: Influence on the Activity of Pt(111) and Iridium Oxide Catalysts in Acidic Media. *Phys. Chem. Chem. Phys.* **2015**, *17*, 8349−8355.
(53) García, G.; Stoffelsma, C.; Rodriguez, P.; Koper, M. T. M. Influence of Beryllium Cations on the Electrochemical Oxidation of Methanol on Stepped Platinum Surfaces in Alkaline Solution. *Surf. Sci.* **2015**, *631*, 267−271.
(54) Previdello, B. A. F.; Machado, E. G.; Varela, H. The Effect of the Alkali Metal Cation on the Electrocatalytic Oxidation of Formate on Platinum. *RSC Adv.* **2014**, *4*, 15271−15275.
(55) Angelucci, C. A.; Varela, H.; Tremiliosi-Filho, G.; Gomes, J. F. The Significance of Non-Covalent Interactions on the Electro-Oxidation of Alcohols on Pt and Au in Alkaline Media. *Electrochem. Commun.* **2013**, *33*, 10−13.
(56) Sitta, E.; Nagao, R.; Kiss, I. Z.; Varela, H. Impact of the Alkali Cation on the Oscillatory Electro-Oxidation of Ethylene Glycol on Platinum. *J. Phys. Chem. C* **2015**, *119*, 1464−1472.
(57) Sitta, E.; Batista, B. C.; Varela, H. The Impact of the Alkali Cation on the Mechanism of the Electro-Oxidation of Ethylene Glycol on Pt. *Chem. Commun.* **2011**, *47*, 3775−3777.
(58) Kodama, K.; Morimoto, Y.; Strmcnik, D. S.; Markovic, N. M. The Role of Non-Covalent Interactions on CO Bulk Oxidation on Pt Single Crystal Electrodes in Alkaline Electrolytes. *Electrochim. Acta* **2015**, *152*, 38−43.
(59) Stoffelsma, C.; Rodriguez, P.; Garcia, G.; Garcia-Araez, N.; Strmcnik, D.; Marković, N. M.; Koper, M. T. M. Promotion of the Oxidation of Carbon Monoxide at Stepped Platinum Single-Crystal Electrodes in Alkaline Media by Lithium and Beryllium Cations. *J. Am. Chem. Soc.* **2010**, *132*, 16127−16133.
(60) Michael, J. D.; Demeter, E. L.; Illes, S. M.; Fan, Q.; Boes, J. R.; Kitchin, J. R. Alkaline Electrolyte and Fe Impurity Effects on the Performance and Active-Phase Structure of NiOOH Thin Films for OER Catalysis Applications. *J. Phys. Chem. C* **2015**, *119*, 11475−11481.
(61) Ding, C.; Zhou, X.; Shi, J.; Yan, P.; Wang, Z.; Liu, G.; Li, C. Abnormal Effects of Cations (Li+, Na+, and K+) on Photo-electrochemical and Electrocatalytic Water Splitting. *J. Phys. Chem. B* **2015**, *119*, 3560−3566.
(62) Thorson, M. R.; Siil, K. I.; Kenis, P. J. A. Effect of Cations on the Electrochemical Conversion of CO2 to CO. *J. Electrochem. Soc.* **2013**, *160*, F69−F74.
(63) Kresse, G.; Furthmüller, J. Efficient Iterative Schemes for Ab Initio Total-Energy Calculations Using a Plane-Wave Basis Set. *Phys. Rev. B: Condens. Matter Mater. Phys.* **1996**, *54*, 11169−11186.
(64) Kresse, G.; Furthmüller, J. Efficiency of Ab-Initio Total Energy Calculations for Metals and Semiconductors Using a Plane-Wave Basis Set. *Comput. Mater. Sci.* **1996**, *6*, 15−50.
(65) Kresse, G.; Hafner, J. Ab Initio Molecular Dynamics for Liquid Metals. *Phys. Rev. B: Condens. Matter Mater. Phys.* **1993**, *47*, 558−561.
(66) Perdew, J. P.; Chevary, J. A.; Vosko, S. H.; Jackson, K. A.; Pederson, M. R.; Singh, D. J.; Fiolhais, C. Atoms, Molecules, Solids, and Surfaces: Applications of the Generalized Gradient Approximation for Exchange and Correlation. *Phys. Rev. B: Condens. Matter Mater. Phys.* **1992**, *46*, 6671−6687.
(67) Blöchl, P. E. Projector Augmented-Wave Method. *Phys. Rev. B: Condens. Matter Mater. Phys.* **1994**, *50*, 17953−17979.
(68) Kresse, G.; Joubert, D. From Ultrasoft Pseudopotentials to the Projector Augmented-Wave Method. *Phys. Rev. B: Condens. Matter Mater. Phys.* **1999**, *59*, 1758−1775.
(69) Monkhorst, H. J.; Pack, J. D. Special Points for Brillouin-Zone Integrations. *Phys. Rev. B* **1976**, *13*, 5188−5192.
(70) Kittel, C. *Introduction to Solid State Physics*, 7th ed.; Wiley: New York, 2008.
(71) Bader, R. F. W. Atoms in Molecules. *Acc. Chem. Res.* **1985**, *18*, 9−15.

DOI: 10.1021/acs.jpcc.5b10979
J. Phys. Chem. C XXXX, XXX, XXX−XXX

(72) Henkelman, G.; Arnaldsson, A.; Jónsson, H. A Fast and Robust Algorithm for Bader Decomposition of Charge Density. *Comput. Mater. Sci.* **2006**, *36*, 354−360.
(73) Sanville, E.; Kenny, S. D.; Smith, R.; Henkelman, G. Improved Grid-Based Algorithm for Bader Charge Allocation. *J. Comput. Chem.* **2007**, *28*, 899−908.
(74) Yeh, K.-Y.; Restaino, N. A.; Esopi, M. R.; Maranas, J. K.; Janik, M. J. The Adsorption of Bisulfate and Sulfate Anions over a Pt(1 1 1) Electrode: A First Principle Study of Adsorption Configurations, Vibrational Frequencies and Linear Sweep Voltammogram Simulations. *Catal. Today* **2013**, *202*, 20−35.
(75) McCrum, I. T.; Akhade, S. A.; Janik, M. J. Electrochemical Specific Adsorption of Halides on Cu 111, 100, and 211: A Density Functional Theory Study. *Electrochim. Acta* **2015**, *173*, 302−309.
(76) Nørskov, J. K.; Rossmeisl, J.; Logadottir, A.; Lindqvist, L.; Kitchin, J. R.; Bligaard, T.; Jónsson, H. Origin of the Overpotential for Oxygen Reduction at a Fuel-Cell Cathode. *J. Phys. Chem. B* **2004**, *108*, 17886−17892.
(77) Reiss, H.; Heller, A. The Absolute Potential of the Standard Hydrogen Electrode: A New Estimate. *J. Phys. Chem.* **1985**, *89*, 4207−4213.
(78) Gomer, R.; Tryson, G. An Experimental Determination of Absolute Half-Cell Emf's and Single Ion Free Energies of Solvation. *J. Chem. Phys.* **1977**, *66*, 4413−4424.
(79) Tsiplakides, D.; Vayenas, C. G. Electrode Work Function and Absolute Potential Scale in Solid-State Electrochemistry. *J. Electrochem. Soc.* **2001**, *148*, E189−E202.
(80) Rostamikia, G.; Janik, M. J. Borohydride Oxidation over Au(111): A First-Principles Mechanistic Study Relevant to Direct Borohydride Fuel Cells. *J. Electrochem. Soc.* **2009**, *156*, B86−B92.
(81) Sakong, S.; Naderian, M.; Mathew, K.; Hennig, R. G.; Groß, A. Density Functional Theory Study of the Electrochemical Interface between a Pt Electrode and an Aqueous Electrolyte Using an Implicit Solvent Method. *J. Chem. Phys.* **2015**, *142*, 234107.
(82) Mathew, K.; Sundararaman, R.; Letchworth-Weaver, K.; Arias, T. A.; Hennig, R. G. Implicit Solvation Model for Density-Functional Study of Nanocrystal Surfaces and Reaction Pathways. *J. Chem. Phys.* **2014**, *140*, 084106.
(83) Karlberg, G. S.; Wahnström, G. An Interaction Model for OH +H2O-Mixed and Pure H2O Overlayers Adsorbed on Pt(111). *J. Chem. Phys.* **2005**, *122*, 194705.
(84) Karlberg, G. S.; Olsson, F. E.; Persson, M.; Wahnström, G. Energetics, Vibrational Spectrum, and Scanning Tunneling Microscopy Images for the Intermediate in Water Production Reaction on Pt(111) from Density Functional Calculations. *J. Chem. Phys.* **2003**, *119*, 4865−4872.
(85) Karlberg, G. S.; Wahnström, G. Density-Functional Based Modeling of the Intermediate in the Water Production Reaction on Pt(111). *Phys. Rev. Lett.* **2004**, *92*, 136103.
(86) Viswanathan, V.; Hansen, H. A.; Rossmeisl, J.; Jaramillo, T. F.; Pitsch, H.; Nørskov, J. K. Simulating Linear Sweep Voltammetry from First-Principles: Application to Electrochemical Oxidation of Water on Pt(111) and Pt3Ni(111). *J. Phys. Chem. C* **2012**, *116*, 4698−4704.
(87) Held, G.; Clay, C.; Barrett, S. D.; Haq, S.; Hodgson, A. The Structure of the Mixed OH+H2O Overlayer on Pt{111}. *J. Chem. Phys.* **2005**, *123*, 064711.
(88) Bedürftig, K.; Völkening, S.; Wang, Y.; Wintterlin, J.; Jacobi, K.; Ertl, G. Vibrational and Structural Properties of OH Adsorbed on Pt(111). *J. Chem. Phys.* **1999**, *111*, 11147−11154.
(89) Clay, C.; Haq, S.; Hodgson, A. Hydrogen Bonding in Mixed OH+H2O Overlayers on Pt(111). *Phys. Rev. Lett.* **2004**, *92*, 046102.
(90) Han, B.; Viswanathan, V.; Pitsch, H. First-Principles Based Analysis of the Electrocatalytic Activity of the Unreconstructed Pt(100) Surface for Oxygen Reduction Reaction. *J. Phys. Chem. C* **2012**, *116*, 6174−6183.
(91) Garcia-Araez, N.; Lukkien, J. J.; Koper, M. T. M.; Feliu, J. M. Competitive Adsorption of Hydrogen and Bromide on Pt(1 0 0): Mean-Field Approximation vs. Monte Carlo Simulations. *J. Electroanal. Chem.* **2006**, *588*, 1−14.
(92) Marković, N. M.; Grgur, B. N.; Ross, P. N. Temperature-Dependent Hydrogen Electrochemistry on Platinum Low-Index Single-Crystal Surfaces in Acid Solutions. *J. Phys. Chem. B* **1997**, *101*, 5405−5413.
(93) Poelsema, B.; Lenz, K.; Comsa, G. The Dissociative Adsorption of Hydrogen on Defect-'Free' Pt(111). *J. Phys.: Condens. Matter* **2010**, *22*, 304006.
(94) Christmann, K.; Ertl, G.; Pignet, T. Adsorption of Hydrogen on a Pt(111) Surface. *Surf. Sci.* **1976**, *54*, 365−392.
(95) Xu, L.; Ma, Y.; Zhang, Y.; Teng, B.; Jiang, Z.; Huang, W. Revisiting H/Pt(111) by a Combined Experimental Study of the H-D Exchange Reaction and First-Principles Calculations. *Sci. China: Chem.* **2011**, *54*, 745−755.
(96) Hanh, T. T. T.; Takimoto, Y.; Sugino, O. First-Principles Thermodynamic Description of Hydrogen Electroadsorption on the Pt(111) Surface. *Surf. Sci.* **2014**, *625*, 104−111.
(97) Gee, A. T.; Hayden, B. E.; Mormiche, C.; Nunney, T. S. The Role of Steps in the Dynamics of Hydrogen Dissociation on Pt(533). *J. Chem. Phys.* **2000**, *112*, 7660−7668.
(98) Gudmundsdottir, S.; Skulason, E.; Weststrate, K.-J.; Juurlink, L.; Jonsson, H. Hydrogen Adsorption and Desorption at the Pt(110)-(1 × 2) Surface: Experimental and Theoretical Study. *Phys. Chem. Chem. Phys.* **2013**, *15*, 6323−6332.
(99) Marković, N. M.; Sarraf, S. T.; Gasteiger, H. A.; Ross, P. N. Hydrogen Electrochemistry on Platinum Low-Index Single-Crystal Surfaces in Alkaline Solution. *J. Chem. Soc., Faraday Trans.* **1996**, *92*, 3719−3725.
(100) van der Niet, M. J. T. C.; den Dunnen, A.; Juurlink, L. B. F.; Koper, M. T. M. A Detailed TPD Study of H2O and Pre-Adsorbed O on the Stepped Pt(553) Surface. *Phys. Chem. Chem. Phys.* **2011**, *13*, 1629−1638.
(101) van der Niet, M. J. T. C.; Berg, O. T.; Juurlink, L. B. F.; Koper, M. T. M. The Interaction between H2O and Preadsorbed O on the Stepped Pt(533) Surface. *J. Phys. Chem. C* **2010**, *114*, 18953−18960.
(102) Petrik, N. G.; Kimmel, G. A. Electron-Stimulated Reactions in Thin D2O Films on Pt(111) Mediated by Electron Trapping. *J. Chem. Phys.* **2004**, *121*, 3727−3735.
(103) Fajín, J. L. C.; Cordeiro, M. N. D. S.; Illas, F.; Gomes, J. R. B. Descriptors Controlling the Catalytic Activity of Metallic Surfaces toward Water Splitting. *J. Catal.* **2010**, *276*, 92−100.
(104) Rossmeisl, J.; Karlberg, G. S.; Jaramillo, T.; Norskov, J. K. Steady State Oxygen Reduction and Cyclic Voltammetry. *Faraday Discuss.* **2009**, *140*, 337−346.
(105) Willard, A. P.; Reed, S. K.; Madden, P. A.; Chandler, D. Water at an Electrochemical Interface-a Simulation Study. *Faraday Discuss.* **2009**, *141*, 423−441.
(106) Ataka, K.-i.; Yotsuyanagi, T.; Osawa, M. Potential-Dependent Reorientation of Water Molecules at an Electrode/Electrolyte Interface Studied by Surface-Enhanced Infrared Absorption Spectroscopy. *J. Phys. Chem.* **1996**, *100*, 10664−10672.
(107) Huzayyin, A.; Chang, J. H.; Lian, K.; Dawson, F. Interaction of Water Molecule with Au(111) and Au(110) Surfaces under the Influence of an External Electric Field. *J. Phys. Chem. C* **2014**, *118*, 3459−3470.
(108) Schmidt, T. J.; Ross, P. N.; Markovic, N. M. Temperature-Dependent Surface Electrochemistry on Pt Single Crystals in Alkaline Electrolyte: Part 1: CO Oxidation. *J. Phys. Chem. B* **2001**, *105*, 12082−12086.
(109) Rodríguez, P.; García, G.; Herrero, E.; Feliu, J.; Koper, M. M. Effect of the Surface Structure of Pt(100) and Pt(110) on the Oxidation of Carbon Monoxide in Alkaline Solution: An FTIR and Electrochemical Study. *Electrocatalysis* **2011**, *2*, 242−253.

DOI: 10.1021/acs.jpcc.5b10979
J. Phys. Chem. C XXXX, XXX, XXX−XXX